Schweizerische Eidgenossenschaft
Confédération suisse
Confederazione Svizzera
Confederaziun svizra

Federal Department of the Environment, Transport, Energy and Communications DETEC

Swiss Federal Office of Energy SFOE
Energy Research and Cleantech Division

Final report dated 01.03.2021

Evaluation of Combined Heat and Power (CHP) Concepts for better Integration into the Future Energy System (Eco-IFES)

Eco-IFES is Task 3.5 of
Renewable Management and Real-Time Control Platform (ReMaP) Project

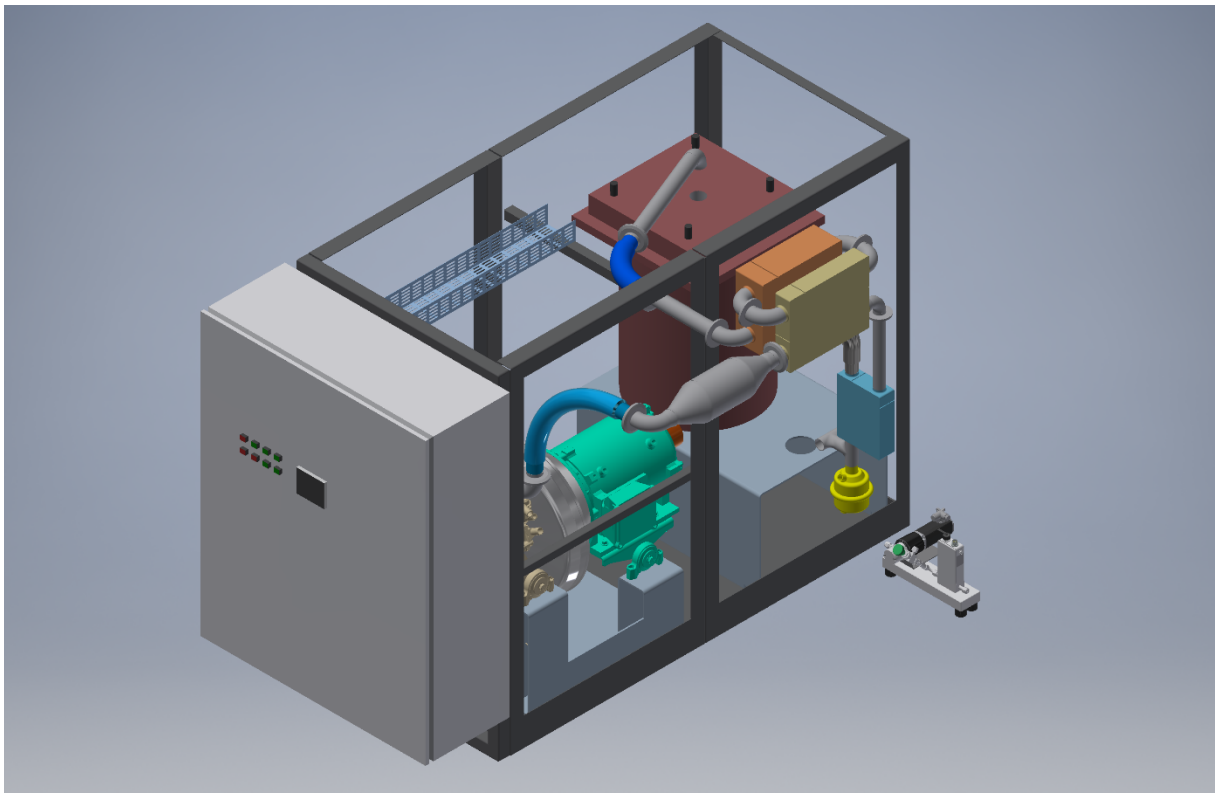

Source: LAV 2020

Date: 01.03.2021

Location: Bern

Publisher:
Swiss Federal Office of Energy SFOE
Energy Research and Cleantech
CH-3003 Bern
www.bfe.admin.ch

Co-Financing:
ETH Zürich Foundation
Weinbergstrasse 29, 8006 Zürich
www.ethz-foundation.ch

ETH Zürich
Rämistrasse 101, 8092 Zürich
www.ethz.ch

Empa
Überlandstrasse 129, 8600 Dübendorf
www.empa.ch

Paul Scherrer Institut
Forschungsstrasse 111, 5232 Villigen
www.psi.ch

smart grid solutions
Pfingstweidstrasse 85, 8005 Zurich
www.smartgridsolutions.ch

Adaptricity
Hohlstrasse 190, 8004 Zurich
www.adaptricity.com

National Instruments Schweiz GmbH
Mellingerstrasse 1, 5400 Baden
www.ni.com

Authors:
Christian Schürch, ETH Zürich, LAV, schuercc@lav.mavt.ethz.ch
Philippe Buchecker, ETH Zürich, LAV, bucheckp@lav.mavt.ethz.ch
Prof. Dr. Konstantinos Boulouchos, ETH Zürich, LAV, boulouchos@lav.mavt.ethz.ch

SFOE project coordinators:
Stephan Renz, info@renzconsulting.ch
Dr. Michael Moser, michael.moser@bfe.admin.ch
Dr. Karin Söderström, Karin.söderström@bfe.admin.ch

SFOE contract number: SI/501810-01

The authors bear the entire responsibility for the content of this report and for the conclusions drawn therefrom.

Zusammenfassung

In ReMaP Task 3.5 werden zwei Optionen zur Flexibilitätssteigerung und Erhöhung der Exergieeffizienz eines konventionellen Blockheizkraftwerkes mithilfe von Simulationen untersucht. Das vielversprechendere Konzept wird in der Folge mit Hardware in the Loop Simulationen und dem Bau eines Prototyps vertieft erforscht. Erste Untersuchungen zeigen, dass ein integriertes Dampfreformer-Konzept gegenüber einer Kombination von BHKW mit Erdspeicher und Wärmepumpe zu bevorzugen ist. Obwohl letzteres die Flexibilität des BHKWs beinahe unbegrenzt erhöhen kann, leidet die Effizienz zu stark unter Wärmeverlusten durch Diffusion im Untergrund. Das Dampfreformer-BHKW Konzept kann den elektrischen Eigendeckungsgrad und die Exergieeffizienz in einer einjährigen Simulation im Vergleich zur konventionellen BHKW Anlage um 30.7%, respektive 8.6% (relativ zum Anfangswert) steigern.

Eine einfache wärmegeführte Betriebsstrategie wird mithilfe von linearisierten Modellen der untersuchten Systeme erweitert und optimiert, wobei das neue Betriebskonzept auch Betriebskosten und den lokalen Strombedarf berücksichtigt. Sowohl für das konventionelle BHKW als auch für das Dampfreformer-Konzept können so die Betriebskosten (um 1.9% / 2.1%) gesenkt und der Eigendeckungsgrad (um 3.8 / 1.7 Prozentpunkte) erhöht werden. Als Kompromiss muss dafür eine Senkung der Exergieeffizienz um 0.23 respektive 0.5 Prozentpunkte in Kauf genommen werden.

Sowohl Hardware- wie auch Softwarekomponenten können erfolgreich in die ReMaP Plattform (Simulation Framework) integriert werden. Die dadurch ermöglichten Hardware in the Loop Experimente mit realen Bedarfsdaten vom NEST Gebäude der Empa zeigen unteranderem, dass das optimierte Betriebskonzept mit der konventionellen sowie mit der Dampfreformer-Ausführung des BHKWs auch in Praxis funktionieren, wenn ein passender Gleitender-Mittelwert-Filter angewendet wird.

Ein Dampfreformer-BHKW Prototyp wird auf Basis des Aladin II BHKWs (siehe [1]) entwickelt und gebaut. Erste Experimente ergeben, dass die gewählten Dampfreformerkomponenten der Kombination von hohen Temperaturen, von bis zu 750°C, und starken Druckpulsationen der Abgase nicht standhalten können. In den Experimenten und der anschliessenden Fehleranalyse werden drei konstruktive und operationelle Verbesserungen des Systems identifiziert.

Résumé

Dans ReMaP Task 3.5, deux options pour augmenter la flexibilité et l'efficacité éxergétique d'une centrale de cogénération classique sont étudiées à l'aide de simulations. Le concept le plus prometteur sera ensuite approfondi grâce à des simulations "hardware-in-the-loop" et à la construction d'un prototype. Les premières investigations montrent qu'un concept de reformeur à vapeur intégré est préférable à une combinaison de la cogénération avec le stockage thermique du sol et la pompe à chaleur. Bien que ce dernier puisse accroître la flexibilité de la cogénération presque indéfiniment, son efficacité souffre massivement des pertes thermiques par diffusion dans le sol. Le concept de la cogénération par reformage à la vapeur peut augmenter l'autosuffisance électrique et l'efficacité éxergétique de 30,7 % et 8,6 %, respectivement, en un an de simulation par rapport au système de cogénération classique.

Une simple stratégie d'exploitation basée sur la chaleur est étendue et optimisée à l'aide de modèles linéaires des systèmes étudiés, et le nouveau concept d'exploitation tient également compte des coûts d'exploitation et de la demande locale d'électricité. Tant pour la cogénération classique que pour le concept de reformeur à la vapeur, les coûts d'exploitation peuvent être réduits (de 1.9 % / 2.1 %) et l'autosuffisance accrue (de 3.8 / 1.7 points de pourcentage). En guise de compromis, une réduction de l'efficacité éxergétique de 0.23 et 0.5 points de pourcentage respectivement doit être acceptée.

Les composants matériels et logiciels sont intégrés avec succès dans la plateforme ReMaP (Simulation Framework). Les expériences "hardware-in-the-loop" avec des données de demande réelle du bâtiment

NEST de l'Empa montrent que le concept d'exploitation optimisé avec la version conventionnelle ainsi qu'avec la version du reformeur à vapeur du système de cogénération fonctionne également dans la pratique, si un filtre à moyenne mobile approprié est appliqué à la demande d'électricité.

Un prototype de reformeur à vapeur est développé et construit sur la base de la cogénération d'Aladin II (voir [1]). Les premières expériences montrent que les composants du reformeur à vapeur choisis ne peuvent pas résister à la combinaison de températures élevées, jusqu'à 750°C, et de fortes pulsations de pression des gaz d'échappement. Les expériences et l'analyse des défaillances qui s'ensuit permettent d'identifier trois améliorations constructives et opérationnelles du système.

Summary

Within ReMaP Task 3.5, two options to improve the flexibility and exergy efficiency of a conventional combined heat and power (CHP) system are investigated with simulations. The more promising option is further tested with hardware-in-the-loop (HIL) experiments on the ReMaP platform. Preliminary simulations show that a steam methane reformer (SMR) CHP concept is to be favoured against the concept of combining the CHP with a ground thermal storage system and a heat pump. Even though the latter has an infinite potential for flexibility, its efficiency suffers massively from thermal losses through diffusion in the ground. Simulations show that over the course of a year, the SMR-CHP concept increases the degree of self-sufficiency in electricity demand by 30.7% and the exergy efficiency by 8.6% relative to the conventional CHP system.

A standard heat-led control concept for conventional CHP systems is improved by also considering economic aspects and using linearized models of the investigated systems to optimize control parameters. For the conventional and the SMR-CHP system, the operating costs are reduced by 1.9% and 2.1% while the degree of electrical self-sufficiency is increased by 3.8 and 1.7 percentage points at the cost of reducing the exergy efficiency by 0.23 and 0.5 percentage points respectively. Both hardware and software components are integrated into the ReMaP platform successfully. Subsequent HIL experiments with real demand data from the NEST building at Empa prove that the optimized control concepts for both the conventional and the SMR-CHP system are working in practice when applying a moving average filter to the electricity demand.

A prototype SMR-CHP plant is sized, designed and built on the basis of the Aladin II mCHP plant (see [1]). First experiments show that the chosen SMR components are not able to withstand the pulsations of the exhaust gases in combination with the very high temperatures of up to 750°C. Three constructive and operational improvements of the system are identified during the experiments.

Main findings

- The combination of CHPs with ground thermal storage is not recommended due to high diffusion rates.
- Over the course of a one-year simulation, a steam methane reformer CHP system promises to be more flexible (increased degree of self-sufficiency by 14.0 percentage points) and exergy efficient (increase of 2.9 percentage points) than a conventional system.
- The chemical and thermal performance of an SMR-CHP system still needs to be validated in a follow-up project, because the chosen components are not able to withstand the rough conditions of a single-cylinder IC engine.
- A hybrid control approach that expands the thermostat control to favour CHP dispatching when the economical break-even point is reached can improve the degree of self-sufficiency and reduce operating costs (by 3.8 percentage points and -1.9% respectively for the conventional CHP).

Contents

Abbreviations

BHE	Borehole Heat Exchanger
CHP	Combined Heat and Power
DSS	Degree of Self Sufficiency (electrical) [2]
ECU	Engine Control Unit
Empa	Swiss Federal Laboratories for Materials Science & Technology
FVM	Finite Volume Method
GUI	Graphical User Interface
HIL	Hardware-in-the-Loop
ICE	Internal Combustion Engine
LAV	Aerothermochemistry and Combustion Systems Laboratory
mCHP	micro Combined Heat and Power (electric output power < 10 kW)
NEST	Next Evolution in Sustainable Building Technologies [3]
NG	Natural Gas
P&ID	Piping and Instrumentation Diagram
PLC	Programmable Logic Controller
PSI	Paul Scherrer Institut
SFW	Simulation Framework
SIA	Swiss Society of Engineers and Architects
SMR	Steam Methane Reformer
TES	Thermal Energy Storage

1 Introduction

1.1 Background Information and Current Situation

Combined heat and power (CHP) plants convert chemical energy, stored in either fossil or renewable fuels, into thermal and electrical energy. Such plants, depending on their size and converter type (internal-combustion engine (ICE), gas turbine, fuel cell, Stirling engine, etc.), can be started up quickly and have great potential to contribute to a stable future energy system based largely on fluctuating renewable energy sources. Conventional combustion-based CHP plants convert exergetically valuable high-temperature heat (at 500 – 700°C) in the exhaust gas to low-temperature heat (at 30 – 80°C). Therefore, a conventional ICE-based micro-CHP (mCHP) plant features a steady-state theoretical exergy efficiency of only 40-60% (depending on its size) although the energetic efficiency can be as high as 100% if condensation in the exhaust takes place.[1] If the high-temperature thermal power was used directly at the available temperatures instead of converting it to low-temperature heat, the exergy efficiency could be improved.

The flexibility of a CHP plant rests on its ability to be started up and shut down quickly and is strongly linked to the heat-demand profile of a consumer and the capacity of the thermal energy storage (TES). The exergy efficiency of a CHP plant and buffer storage combination with a given heat-demand profile is not only dependent on the steady-state exergy efficiency of the CHP plant, but also on the storage capacity and its thermal losses. If further components are necessary to extract heat from the storage (e.g., a heat pump to extract heat from a borehole), the efficiencies of these components and the temperature levels of the fluids need to be considered, too.

As CHP plants could play an important role in future energy systems, it is the overall goal of this project to find a way to increase both exergy efficiency and flexibility of such plants. Additionally, the ability to store energy seasonally shall be investigated. The focus in this project lies on mCHP plants with an electrical output power of below 10 kW but the developed concepts should also be able to suit bigger plants to a certain extent.

1.2 Purpose of the Project

To reach the main goal of simultaneously increasing flexibility and exergy efficiency, two concepts are suggested, where one mainly focuses on flexibility and another is primarily aimed at increasing the exergy efficiency. Further investigations shall then show which of the two concepts performs better in both criteria and has the better potential for seasonal energy storage. Both concepts are illustrated in Figure 1.

Concept 1: Using a ground thermal storage as heat buffer for a CHP plant leads to an almost infinitely big storage capacity. Combining such a borehole heat exchanger (BHE) with a CHP plant and a heat pump gives the operator the freedom of operating the CHP whenever the electricity price is favourable. The produced heat can either be used for satisfying a heat sink directly or it can be stored in the BHE for later use. The heat pump can be used to consume electrical power from the grid if heat is requested but electricity prices are too low to profitably operate the CHP.

Concept 2: The exergy loss of the high-temperature heat of the exhaust gas is the biggest contributor to the overall exergy loss in the CHP system. Therefore, this concept features a chemical conversion process that consumes part of the high-temperature heat of the exhaust gas. A steam methane reformer (SMR) process requires high temperatures and produces syngas from methane and steam. The process reactor sits right between the three-way catalytic converter and the exhaust heat

[1] CHP and heating manufacturers provide energy efficiencies based on the lower heating value (LHV). For natural gas, the higher heating value is roughly 10% higher than the LHV, therefore the energy efficiency could potentially add up to 110% for a lossless process and complete condensation.

exchanger of the CHP plant. The syngas can be stored in the gas grid seasonally and features a high exergy content. Because the SMR process consumes some of the heat, the total heat production of such an SMR-CHP is reduced. At times of very high heat demand, the SMR process could be turned off in order to extract full thermal power from the CHP.

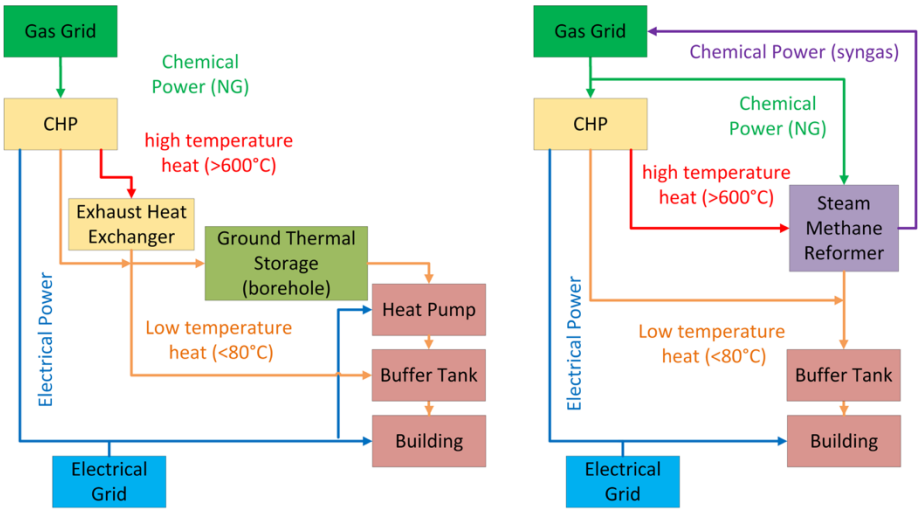

Figure 1: In concept 1 (on the left) a ground thermal storage increases the flexibility of the CHP almost infinitely, while concept 2 (on the right) mainly focuses on increasing the exergy efficiency of the system by making direct use of the high-temperature heat in a steam methane reformer.

1.3 Objectives

In a first step, simulations and feasibility studies serve as a basis for the decision which of the two concepts described in Section 1.2 is more promising. An experimental test rig of the prevailing concept will therefore be built in a second step. The test rig will be installed and operated to demonstrate the theoretical findings. The starting point for the experiment is an existing mCHP plant with 7 kW electrical power, highest in-class electrical efficiency of >30% and minimized cold-start emissions. This prototype plant was developed within the framework of the SFOE R&D project Aladin II [1].

Along with installing the CHP plant in the small engine laboratory of LAV / ETHZ, a connection of this plant to the ReMaP Simulation Framework (SFW) shall be established. This will allow sample energy systems to be put together where the CHP acts in combination with other hardware components or computer models of other components. An operation strategy will be developed and implemented into a controller, which will be running in the SFW to control all included hardware and software components.

Finally, experiments where the CHP and other real or modelled components are combined will demonstrate the performance of the concept and its operation strategy. These experiments shall also confirm the validation of the models used for simulations.

2 Procedures and Methodology

As described in Section 1.3, Task 3.5 of the ReMaP project is focused on the expansion and improvement of the mCHP concept, for which the Aladin II mCHP plant, which had been developed in preceding projects [1] [4] [5] , serves as a testbed. Both a physical prototype (Section 2.1) and a detailed Matlab/Simulink model of the plant (developed at the Institute for Dynamic Systems and Control (IDSC), ETH Zürich; Section 2.2) are adopted from the aforementioned sources and form the foundation for all investigations presented in this report.

2.1 Conventional CHP Plant

The mCHP consists of a single cylinder natural gas (NG) ICE, a water-cooled generator, a high-efficiency exhaust gas cooler and the necessary cooling circuits. This configuration is referred to as the conventional CHP plant throughout this report and is used for all hardware-in-the-loop (HIL) experiments with the ReMaP simulation framework (SFW) as described in Section 2.7.6 and 3.5. Figure 2 shows the power flow schematic of the installed conventional plant. It sources NG from the gas grid and converts this chemical into electrical and thermal power. The electric power output is 7 kW, while approximately 11.7 kW thermal power is produced in steady state. The internal combustion engine has no throttle and is always operated at a nominal 3000 rpm and full load. A technical schematic of the plant can be found in appendix 8.1, Figure 32 and the machine itself is described in more detail in the final report of the Aladin II R&D Project [1].

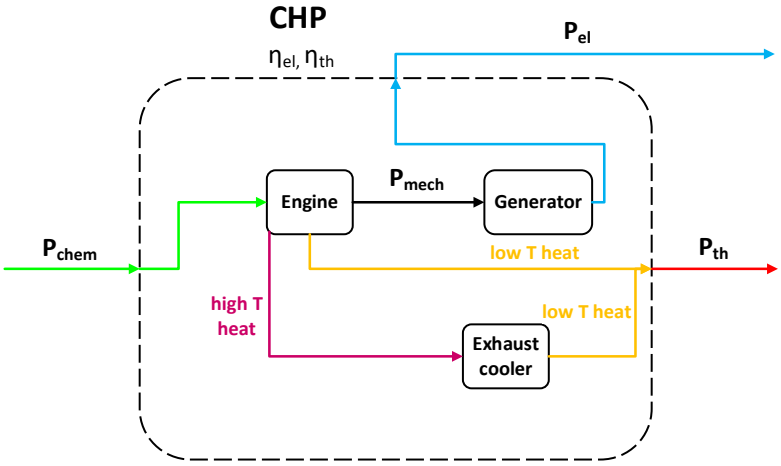

Figure 2: Power flow schematic of the conventional CHP plant. The high-temperature heat in the exhaust gases is extracted in the exhaust gas cooler and added to the engine cooling circuit. Both together add up to the thermal power output of the plant.

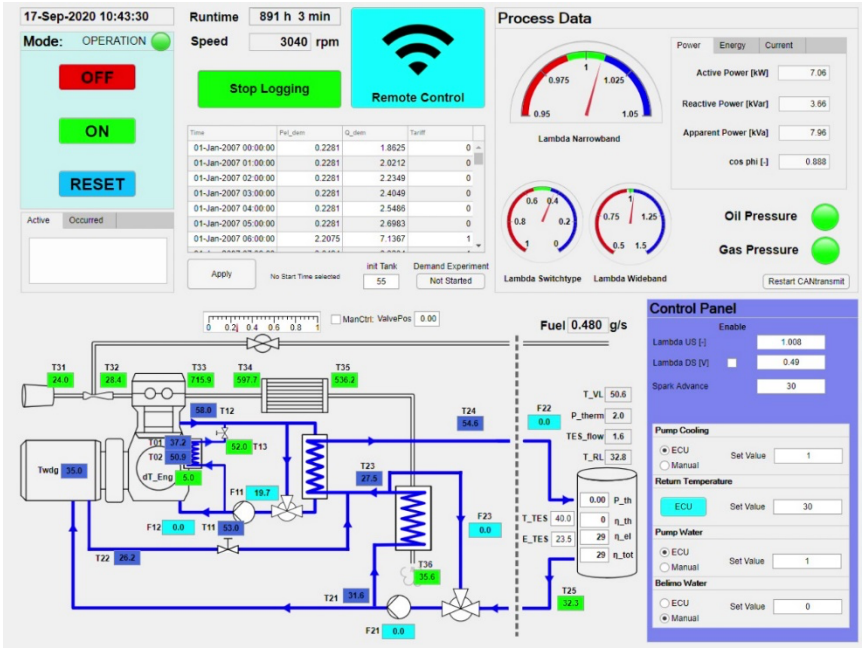

Figure 3: GUI of the CHP plant. In the middle at the top, the operator can allow for remote control access via the SFW.

The engine control unit (ECU) controls the generator, the engine and all pumps and valves of the plant. The ECU also takes care of the local error handling and makes sure the machine operates in a save way, regardless of external control commands. The graphical user interface (GUI), is shown in Figure 3, allows the user to observe all measured quantities and the status of the machine. In the GUI, the machine can be started and stopped manually or remote-control access can be given to the ReMaP SFW for HIL experiments.

2.2 CHP Model

For preliminary investigations and CHP simulations, a Matlab/Simulink model is adapted from preceding projects [5] [1]. It is reworked to suit the needs of Task 3.5 and validated using measurements from the Aladin II prototype plant in its current state.

The model is zero-dimensional and models temperatures as well as heat and mass flows both within and between different components, while pressure changes are neglected. An overview of the model structure and the represented components can be found in Figure 4. It is set up for simulations with a long timespan (one year) with its main outputs being time-resolved electrical and thermal power production saved at 60-second intervals. The plant scheduling is handled by the operation controller (Figure 4, orange box, top left) based on user supplied heat and electricity demand data and the state of an internal, simplified TES model. The control logic is described in Section 2.6.

The engine's performance is modelled using the Willans approximation, a constant nominal fuel mass flow (when the engine is running) and a fixed generator efficiency leading to a constant nominal electrical power output. The short start-up dynamics of the mechanical power output—in the order of 30 seconds—is hence neglected. The thermal behaviour of the ICE and the rest of the CHP plant is modelled in more detail, allowing thermal power dynamics of the real plant to be reproduced in the model.

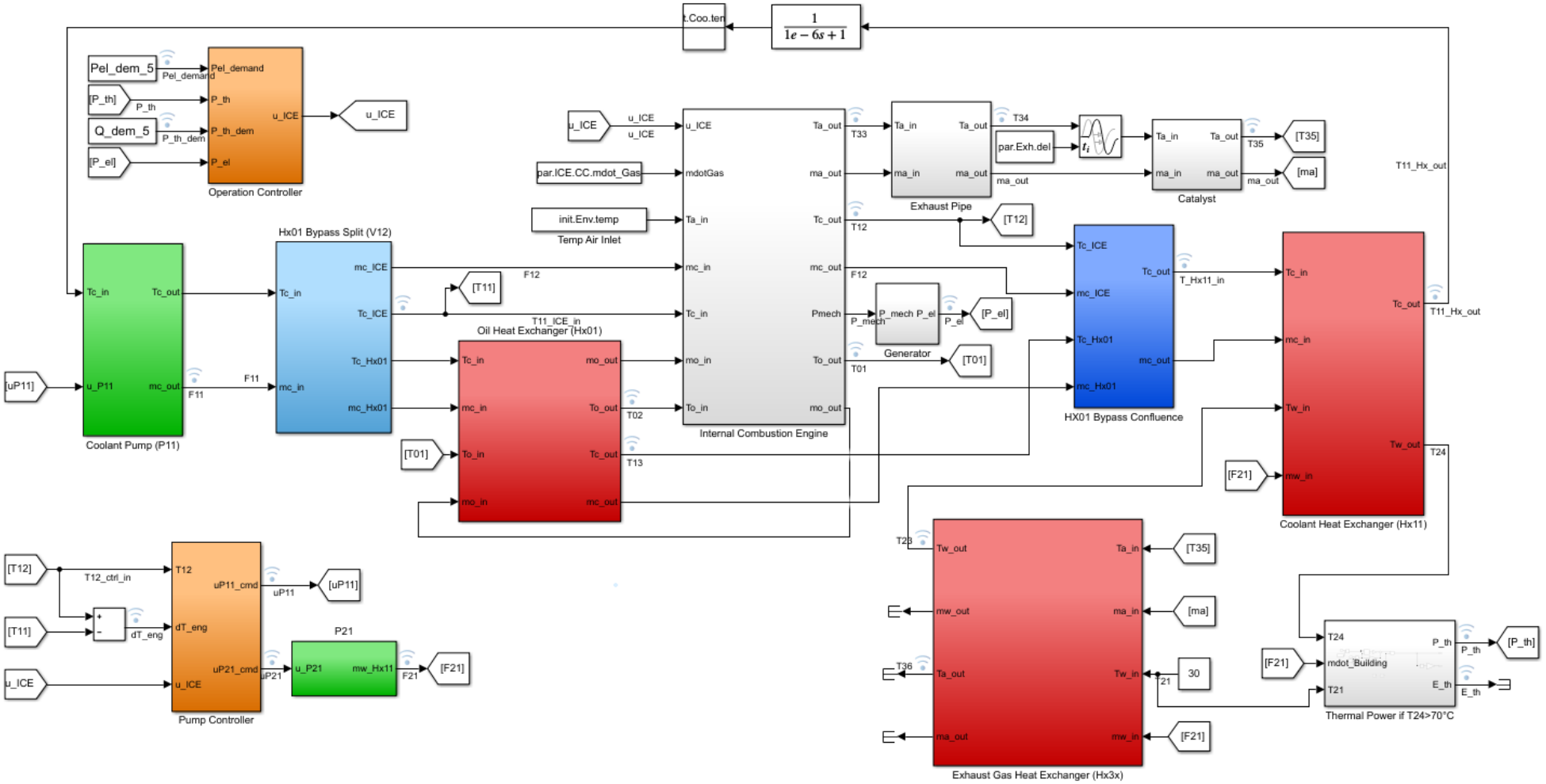

Figure 4: Simulink model of the conventional CHP plant. Red blocks: heat exchangers; green blocks: pumps; blue blocks: valves; grey blocks: ICE and exhaust; orange blocks: controller modules.

2.2.1 Thermal Energy Storage Model

In analogy to literature [6] [7] [8], a simplified zero-dimensional TES model is integrated into the CHP plant for long-term simulations. It is also available as a stand-alone for SFW integration. The energy storage level variable is calculated using a simple energy balance (Equation 1) including CHP thermal power output $P_{th,CHP}$, heat demand Q_{dem} (i.e., from a building) and a heat loss term. The heat loss term consists of the overall heat transfer coefficient $\left(U = 1.21 \frac{W}{Km^2}\right)$, the total heat transfer area $(A_{TES} = 10.38\, m^2)$ and the difference between TES temperature T_{TES} and ambient temperature $(T_{amb} = 23°C)$.

$$\frac{dT_{TES}}{dt} = P_{th,CHP} - \dot{Q}_{dem} - UA_{TES} \cdot (T_{TES} - T_{amb}) \qquad \text{Equation 1}$$

According to Vögelin [7], the TES is sized to buffer ten hours of CHP operation at nominal power resulting in a storage capacity of 117.3 kWh. The return temperature is assumed to be constant at 30° Celsius over the entire operating range ($T_{TES} \in [30°C, 80°C]$).

2.3 Evaluating System Expansion Concepts

Preliminary investigations using simulations are undertaken to assess the performance potential of each system expansion concept (Figure 1, Section 1.2). These form the basis on which a decision to move forward with one of the concepts—including the construction of a prototype—can be made. These investigations are focused on characterising the behaviour of added components (borehole heat exchanger for Concept 1, steam reformer for Concept 2) and assessing their technical potential within the CHP system.

2.3.1 Evaluating Concept 1

Concept 1 explores the benefits of adding a borehole heat exchanger and ground source heat pump setup to the existing CHP layout. The addition of a single borehole with a double U-tube design, a depth of 260 m and an internal pipe diameter of 40 mm is hence investigated. The borehole configuration is based on an existing unit at Empa's energy hub [9] [10].

The borehole heat exchanger was modelled and validated by Gerber [10] in a semester project within ReMaP Task 3.5. The model was validated using data of an extended thermal-response test that had been performed at the time of installation [9]. To be able to capture the borehole behaviour with sufficient accuracy, it is largely modelled in 2D using the finite-volume method. Due to rotational symmetries of the soil, the tangential direction is neglected. To model the fluid, a discretisation in the z-direction is sufficient, with heat transfer between the four pipes and the soil being lumped together. The model interfaces are such that it returns a time-resolved outlet temperature for a given inlet mass flow and temperature.

Using this computational fluid dynamics (CFD) borehole model with CHP relevant charging and discharging conditions is found to give enough information about the borehole's seasonal storage potential and the benefits of a combined CHP-BHE system to analyse the potential of Concept 1.

2.3.2 Evaluating Concept 2

For the evaluation of Concept 2, the SMR is linked to the CHP model's exhaust system via a heat exchanger, which is used to raise the necessary steam for the methane reforming process. The chemical reaction then takes place in a catalytic reactor that is integrated into the last section of the heat exchanger. The initial evaluation of the concept focusses on a steady-state exergy analysis to quantify the achievable second law efficiency increase from integrating an SMR into the CHP system.

The reaction kinetics of the SMR reactor are investigated using ANSYS Chemkin-Pro 19.2. The reaction mechanism used is a methane reforming process in a flow reactor coated with nickel and was developed by a research group of the Karlsruhe Institute of Technology [11]. The reaction kinetics and the optimal

SMR integration method have been examined for ReMaP Task 3.5 during a semester project by Croce [12]. The conversion efficiency—as a result of these reaction kinetic investigations—is used for the initial evaluation of Concept 2. For subsequent investigations, the conversion efficiency is taken from the sizing documents of the reactor manufacturer (see Section 2.5.1).

The chemical exergy rates are calculated using the conversion rates from the above-mentioned chemical calculations and Equation 2 for the chemical exergy of gas mixtures ($e_{x,mix}$) [13]. The chemical exergy of the mixture is calculated by summing the chemical exergy of components *i* ($e_{x,i}$) (weighted by their corresponding molar fractions x_i) and subtracting the entropy of mixing, where *R* is the universal gas constant and T_0 is the standard temperature. Pure fuels are taken into account by multiplying their chemical energy content with a quality factor [8], electric energy is assumed equal to exergy, while thermal energy is converted to exergy using the Carnot efficiency [14].

$$e_{x,mix} = \sum_i (x_i e_{x,i}) + RT_0 \sum_i (x_i \ln x_i) \qquad \text{Equation 2}$$

2.4 SMR-CHP Plant

The conventional CHP is modified with a package of three additional heat exchangers, which are inserted into the exhaust gas path of the conventional CHP plant between the catalytic converter and the exhaust gas heat exchanger as part of the SMR process. This configuration was in operation only a few hours due to a failure of the reformer heat exchanger. The few results that could be obtained from this configuration and a failure analysis are described in Section 3.2.

2.4.1 Working Principle

The SMR-CHP plant is based on the conventional CHP plant and features an extra SMR module in the high temperature exhaust path as shown in Figure 5. This module converts natural gas and superheated steam into syngas using the high-temperature thermal power provided by the exhaust gas. The remaining heat in the exhaust gas is recovered in the already existing exhaust gas cooler.

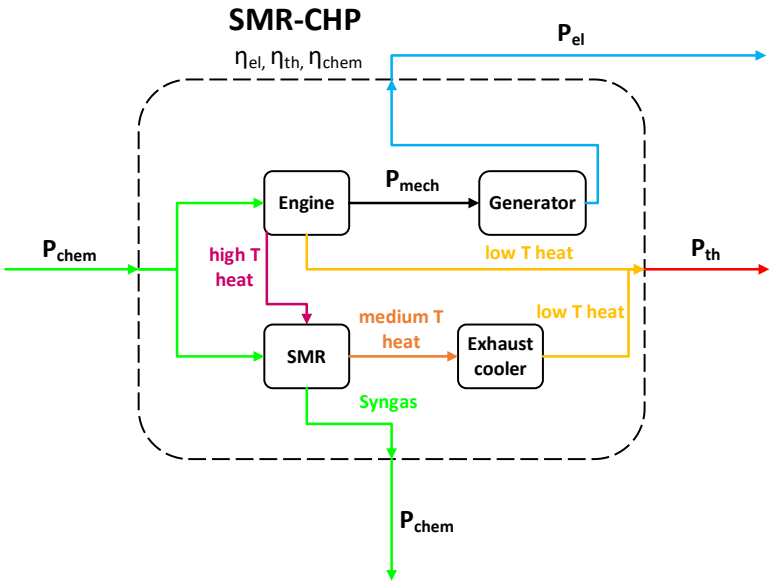

Figure 5: Power flow schematic of the SMR-CHP plant. The SMR converts natural gas and superheated steam to syngas while consuming high temperature heat.

Technically, the SMR module consists of three heat exchangers, as shown in Figure 6: The pre-heater (E-401) preheats and partially evaporates the demineralized water while recovering the heat of the hot syngas exiting the reformer (E-101). In the super-heater (E-102), the partially evaporated water is completely evaporated and superheated. After the superheated steam exits the super-heater, methane is admixed. The reformer is the key component and is catalytically coated on the secondary side, where the steam-methane mixture enters the reactor. The hot exhaust gas coming from the engine enters the secondary side of the reformer to provide the heat necessary for the reformer reactions (1) and (2):

$$Reforming\ (1): \qquad CH_4 + H_2O \leftrightarrow CO + 3\,H_2 \qquad \Delta H_r = 206\frac{kJ}{mol}$$

$$Water - Gas\ Shift\ (2): \qquad CO + H_2O \leftrightarrow CO_2 + H_2 \qquad \Delta H_r = -41\frac{kJ}{mol}$$

According to the vendor of the reactor, the wet syngas exiting the reformer is composed of roughly 58% water vapour, 24% hydrogen, 12% methane, 6% carbon dioxide and some carbon monoxide at the expected conditions (all values given in molar fractions). After cooling the syngas down and letting the water condensate out, the dry composition is expected to be 58% H_2, 27% CH_4, 14% CO_2 and 1% CO. To measure the composition of the product stream, a gas chromatographer is installed after an additional syngas cooler. The mass flow is calculated using the controlled and measured input mass flow of the methane and demineralized water. A detailed piping and instrumentation diagram (P&ID) of the complete process can be found in Appendix 8.2.

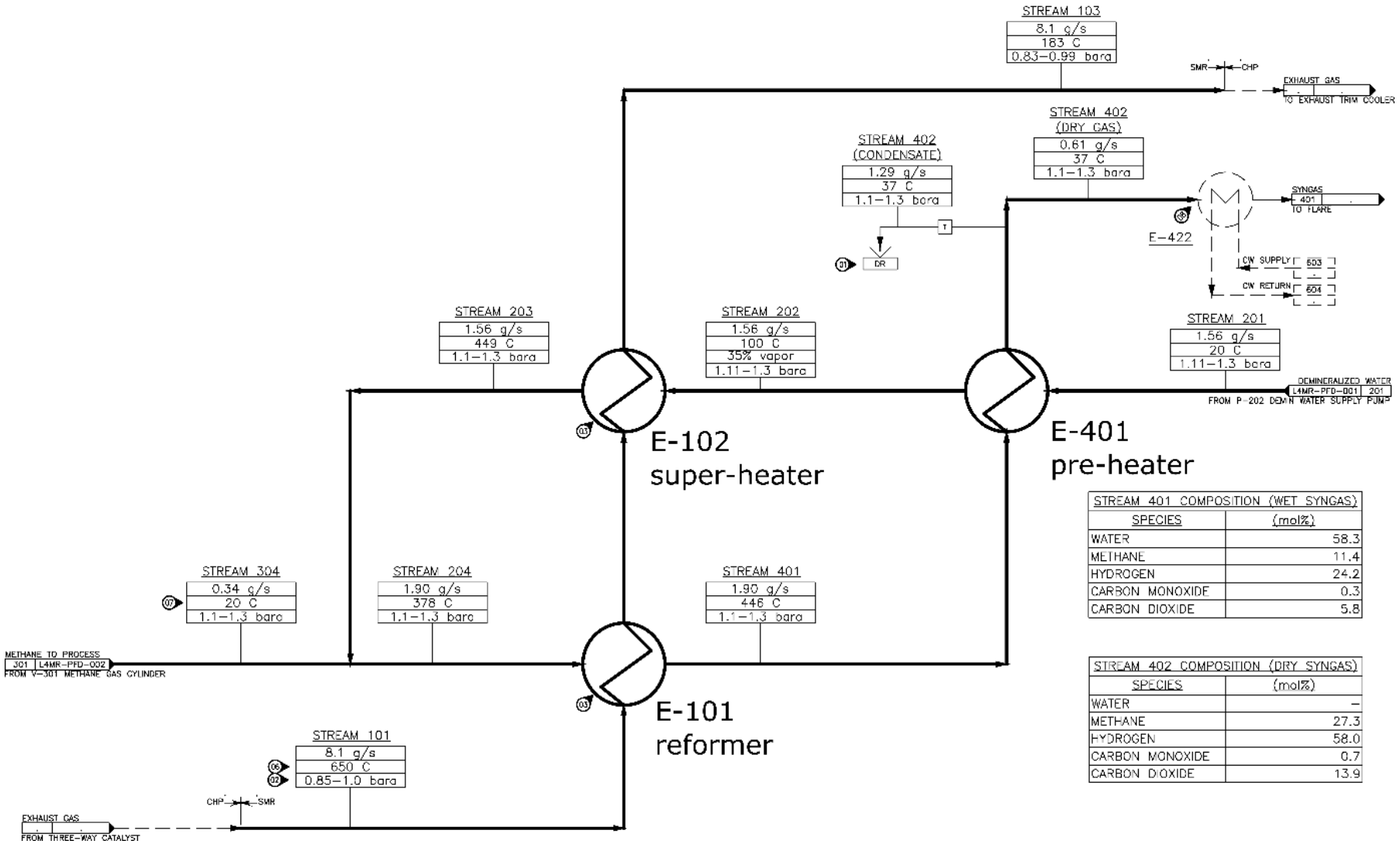

STREAM 401 COMPOSITION (WET SYNGAS)	
SPECIES	(mol%)
WATER	58.3
METHANE	11.4
HYDROGEN	24.2
CARBON MONOXIDE	0.3
CARBON DIOXIDE	5.8

STREAM 402 COMPOSITION (DRY SYNGAS)	
SPECIES	(mol%)
WATER	–
METHANE	27.3
HYDROGEN	58.0
CARBON MONOXIDE	0.7
CARBON DIOXIDE	13.9

Figure 6: Schematic of the SMR process. All flow and temperature values correspond to the design steady state point

2.4.2 Plant Design and Manufacturing

The whole SMR process has to be sized such that the thermal power consumption is appropriate to the Aladin II CHP exhaust gas enthalpy flow. As the reaction temperature is key for the chemical conversion rate, the process temperatures are also defining boundaries for the maximum reactant mass flow rates. Given the temperature after the catalytic converter (650 – 750 °C) and the exhaust gas mass flow, the reformer manufacturer Bosal (https://eci.bosal.com/) sized the three heat exchangers E-101, E-102 and E-401 (see Figure 6) accordingly. All design parameters as provided by Bosal are listed in Table 1.

Table 1: Sizing parameters as provided by Bosal.

Parameter	*Value*	*Units*
Cold H_2O mass flow	1.56	g/s
Cold CH_4 mass flow	0.34	g/s
T_{H2O} @ inlet of E-401	20	°C
T_{H2O} @ exit of E-401	100	°C
Vapour fraction @ exit of E-401	35.4	%
T_{Syngas} @ inlet of E-401	446	°C
T_{H2O} @ exit of E-102	449	°C
T_{mix} @ inlet of E-101	378	°C
Hot exhaust gas mass flow	8.10	g/s
$T_{exhaust}$ @ inlet of E-101	650	°C
$T_{exhaust}$ @ exit of E-102	138	°C
CH_4 conversion	35.0	%

The system components are integrated in the existing exhaust gas path of the Aladin II CHP plant using 3D-CAD software. All manufacturing, welding and installation work is done in-house, at the LAV mechanical workshop. The control cabinet for the SMR process is designed and built in the LAV electronic workshop. All wiring in the laboratory is done in-house as well.

Figure 7 shows the exhaust path of the SMR-CHP; the prismatic reactor heat exchanger E-101 is connected directly to the catalytic converter of the engine. The super-heater E-102 is connected to E-101 and the pre-heater E-401 sits below in the back. Figure 8 shows the CAD render and a photograph of the installed complete plant. The cylindrical big exhaust gas heat exchanger is shown in ruby colour and sits in the back left corner of the plant. In Appendix 8.2 a detailed P&ID of the SMR process can be found.

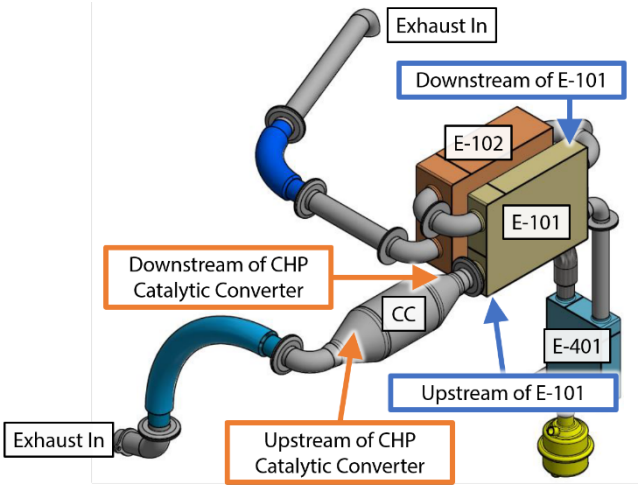

Figure 7: CAD render of the SMR-CHP exhaust path including the catalytic converter (CC) and the three heat exchangers for the SMR process.

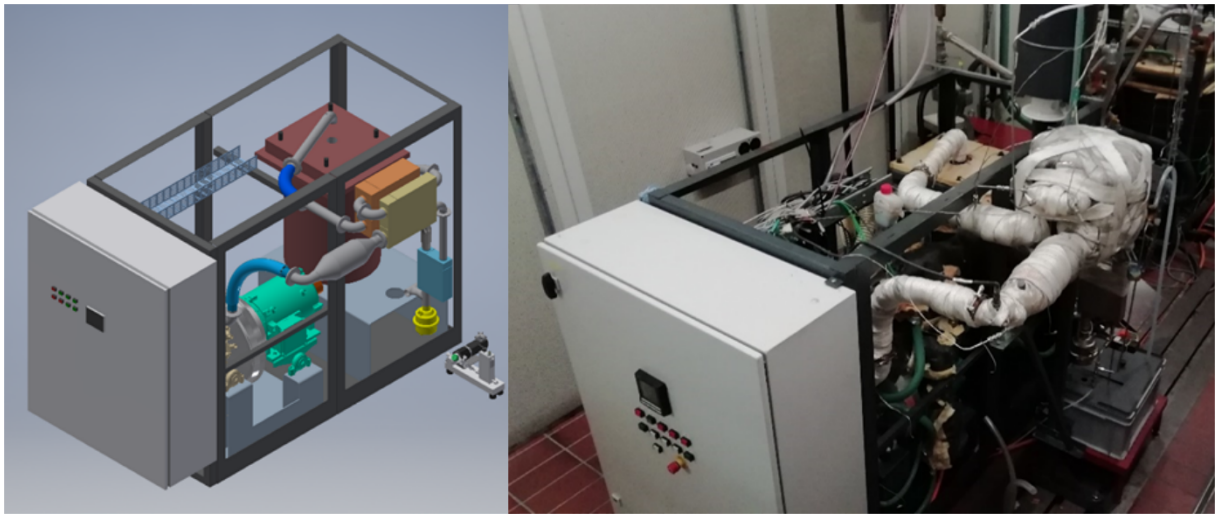

Figure 8: SMR-CHP plant as CAD render (left) and the physical plant as it was installed in the LAV engine lab (right).

2.4.3 Control System

An overall control system is running on a programmable logic controller (PLC), which receives all system information about pressure, temperature, valve positions and flows. All set values are generated on the PLC according to the rules described below. A GUI allows the user to observe the process and adjust operating parameters. The GUI is shown in Figure 9 and Figure 10. A safety control loop checks all sensor values and displays a warning once the lower or higher warning limit is reached. At lower or higher alarm limit, the PLC triggers an emergency stop; all flow set values are set to zero but the CHP continues running. Only if the pressure low or high alarm limit is reached, the CHP is also turned off as both situations could damage system components or pose the risk of an uncontrolled syngas. The control system is technically defined by LAV and finally programmed on the PLC by the ehub group at Empa, Dübendorf.

To ensure mechanical integrity of the heat exchangers, the pressure on the syngas side must be higher than on the exhaust side at all times. To ensure this requirement is fulfilled, the pressure is hysteresis controlled; if the upper pressure limit is reached, a magnetic flow valve (FS-405, see P&ID in Appendix

8.2) opens and stays open until the lower pressure limit is reached. A manually adjustable flow limiter defines the maximum flow rate such that at the steady state, the pressure control valve does not cycle. The pressure control loop is always active, regardless of the system status. A spring-loaded pressure safety valve prevents over-pressurization.

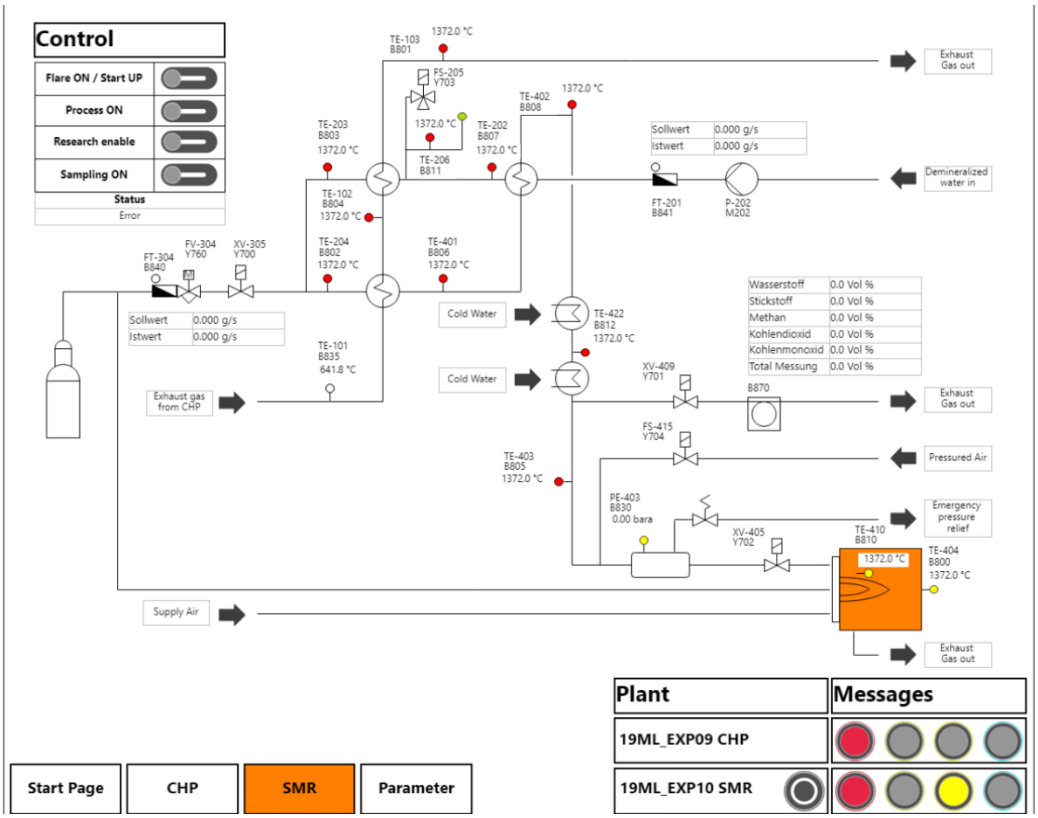

Figure 9: GUI of the SMR controller, implemented by the ehub group at Empa, Dübendorf. On the "SMR" tab, the whole process can be surveyed.

Separate devices control the flows of both methane and water with internal PID controllers but these flow controllers receive their set values from the PLC. Figure 11 shows the look-up table for the water mass flow set value. Once the exhaust gas temperature exceeds t0, this map becomes active. All parameters f1, f2 and t0 – t2 can be adjusted in the GUI. The flow rate set value for methane is defined by the steam to fuel ratio, which is also an adjustable parameter in the GUI. Temperatures are not controlled actively but influenced by the flow rates.

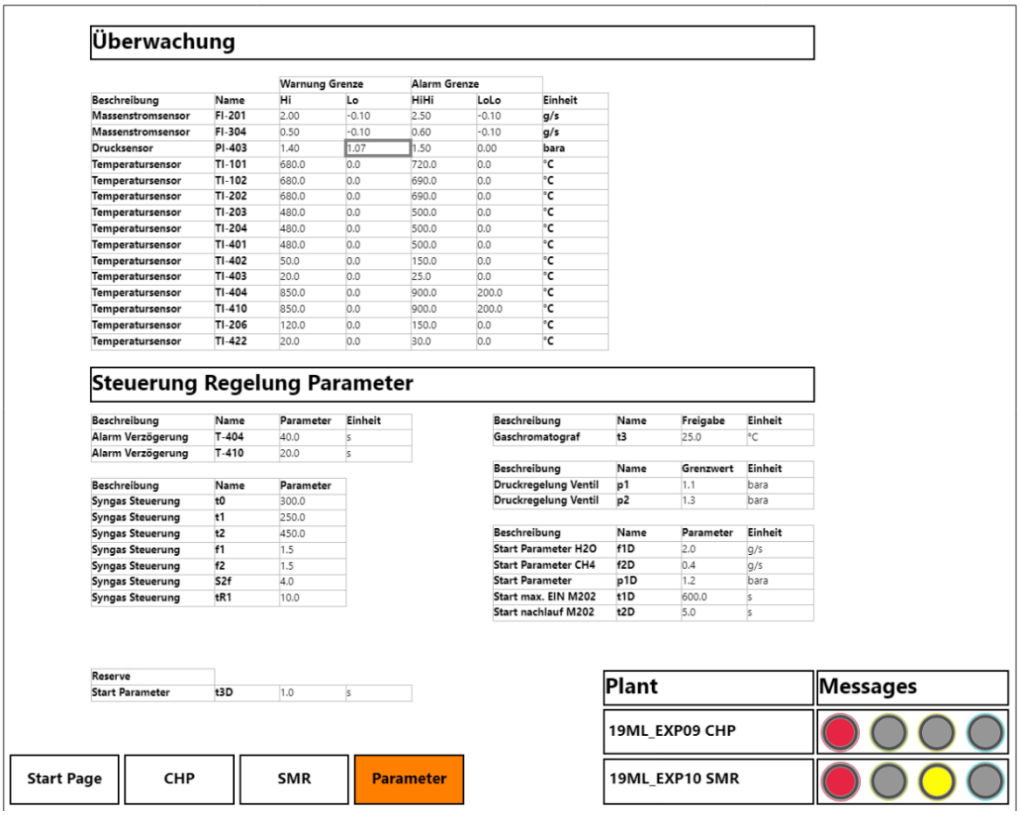

Figure 10: GUI of the SMR controller. All control parameters are set on the "Parameter" tab.

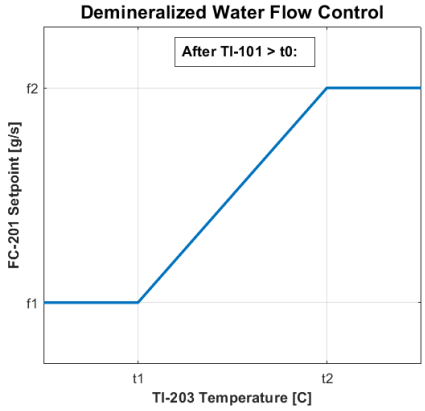

Figure 11: The water flow rate set value is based on temperature TI-203, the steam temperature after the evaporator, once the exhaust gas exceeds t0. The parameters f1, f2, t0, t1 and t2 can be adjusted in the GUI.

2.5 Quantifying Long-Term Effects of Concept 2

To assess the impact of SMR integration on the CHP system performance, simulations with a timeframe of one year are run for both the conventional CHP configuration and the SMR-CHP layout. This process

involves building a SMR Simulink model and incorporating it into the standard CHP model as well as finding appropriate demand data and evaluation criteria to judge each layout's performance.

2.5.1 Steam Methane Reformer Model

The SMR model is a grey-box model based in part on the steady state input/output behaviour of the pure steam methane reformer design that was developed in cooperation with Bosal ECI and based on the findings of the initial investigation by Croce [12]. The model is updated using findings and insights from the experimental data obtained during commissioning of the SMR prototype, as compiled in the student project by Sapkota. [15] Due to the limited availability of data, the model is not validated. Figure 12 shows an overview of the SMR Simulink model. The SMR model consists of five major components. These are (from top left to bottom right):

1. The heat exchanger network, modelling the heat transfer from the exhaust to SMR reactants. Based on early prototype data, a constant heat transfer rate ($\dot{Q}_{SMR,in}$) is found to be a good approximation of cold-start and steady state SMR operation. (When the SMR is offline, no heat is exchanged.) The exhaust gas outlet temperature is calculated according to the general equation: $\frac{1}{m \cdot c_p}\frac{dT_{out}}{dt} = (T_{in} - T_{out}) \cdot c_p \cdot \dot{m} - \dot{Q}_{in,SMR}$ where the time-derivative term is included to prevent discontinuities when the steam reformer is switched on or off. The mass *m* represents an estimate for the mass of exhaust gas inside the SMR during operation.
2. The "Hx3x Observer", modelling the CHP's exhaust cooler to provide an accurate estimate of the SMR's impact on thermal power output. The difference in thermal power output is calculated by comparing the water outlet temperature of the CHP's exhaust cooler and the one being modelled within the SMR (which is fed with lower exhaust temperatures due to the SMR reaction process). This is necessary to allow the SMR model to be used for HIL simulations with the CHP prototype plant, as the actual inlet temperature of the exhaust cooler cannot be influenced by the simulation.
3. The water controller, regulating the steam mass flow using a lookup based on experimental data for cold-start behaviour.
4. The "methane switch" models the fuel valve, injecting the appropriate amount of methane for a fixed steam-to-fuel ratio. Injection starts at 94% nominal steam mass flow.
5. The SMR chemical reactor, calculating the product mass flow, composition and ΔP_{chem} (the amount of thermal energy converted to chemical energy) based on the input mass flow and fixed nominal conversion rates. The performance data of the SMR was provided by the manufacturer Bosal as a result of the sizing and quotation process.

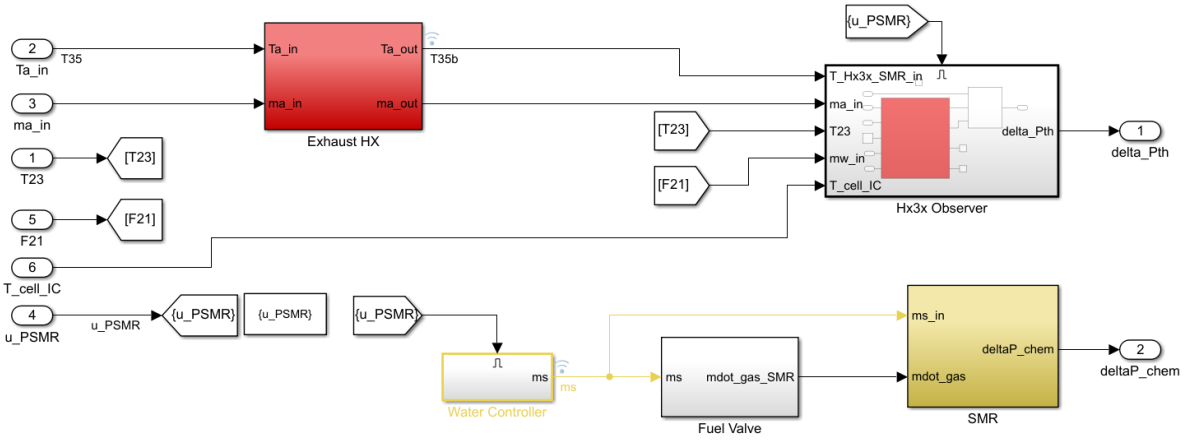

Figure 12: SMR Simulink model overview.

2.5.2 Integration into CHP Model

The steam reformer is integrated into the exhaust path of the CHP between the catalytic converter and the exhaust gas cooler.

Table 2: Key characteristics of SMR model performance. Values based on steady state calculations.

Parameter	*Value*	*Units*
$P_{th,SMR-CHP}$[2]	6741	W
ΔP_{chem}	1934	W
$P_{loss,SMR}$ [12]	580	W
$\dot{Q}_{in,SMR}$	5528	W
$\dot{m}_{H_2O,in}$	1.6	g/s
$\dot{m}_{CH_4,in}$	0.35	g/s
$\dot{m}_{H_2,out}$	0.062	g/s

As long as the CHP's exhaust temperature is high enough[3], SMR operation can be controlled (switched on or off) independently of the CHP plant. When in operation, the plant's thermal output power drops to 6.74 kW. Appropriate control mechanisms for switching the steam reformer on and off are integrated into the CHP model's operation controller and will be discussed in Section 2.6.1. Overall, changes to integrate the SMR model are minor.

2.5.3 Demand Data

Heat and electricity demand profiles are provided by Empa and have been calculated based on residential buildings in the city of St. Gallen using Empa's in house calculation tool CESAR [16]. The data was calculated based on building physics and typical weather data, while electricity and domestic hot water demand profiles were calculated according to SIA norm 2024 schedules [17]. Data for a single-family home with two residents and a heated floor area of 242 m^2 is used in this study. The domestic hot water and space heating demands are lumped together. Table 3 summarizes the demand data.

Table 3: Demand data information.

	Sum over a year	*Mean*	*Max*
$P_{el,dem}$	14 MWh	1.6 kW	4.05 kW
Q_{dem}	30.1 MWh	3.4 kW	18.6 kW

2.5.4 Evaluation Criteria

The main constraint for the systems is the need to cover the local heating demand completely (i.e., there is no backup boiler installed on the premises). Systematic heat rejection to the environment is not allowed, although some heat losses are inevitable. The evaluation criteria are:

[2] CHP thermal power output when the SMR is in operation. When the SMR is off, thermal power output is the same as conventional CHP output.

[3] Operation requires an exhaust gas temperature of at least 550°C after the catalytic converter.

1. Satisfying 100% of the heating demand is critical, since no backup heating system is considered in the evaluation. Solutions that fail to satisfy this criterion are not taken into further consideration.
2. The second law efficiency (ε) of the system is the key performance criterion. Exergy efficiency is a good measure for comparing conversion processes involving different forms of energy [8], taking into account, for example, the difference in "usefulness" of heat provided at different temperature levels.
3. The fraction of the electricity demand covered by CHP operation (i.e., degree of self-sufficiency, DSS [2]) is chosen as a good indicator of plant flexibility and to what degree heat generation can be decoupled from heat demand.
4. Operating costs are also taken into consideration in a simplified form. Since the size of the CHP and all additional shared components are identical for all configurations, and the SMRs early prototype status makes an accurate prediction of its commercial costs difficult, investment and maintenance costs are not considered. Nevertheless, it is believed that running costs are a useful parameter to evaluate performance and flexibility of different configurations. They are sensitive to heat losses (i.e., first law efficiency), unfavourably timed electricity production, and excessive engine running hours.

Operating costs are calculated based on 2019 electricity pricing schemes for private household consumers in the city of Zürich [18]. The gas price of 9.59 Rp./kWh is taken from natural-gas supplier energie360° [19]. It is assumed that the SMR produced methane and hydrogen mixture can be sold back to the national gas grid[4] at the normal, heating-value based, gas price.

2.6 Operation Strategy Development

Combined heat and power plants generally have the possibility to operate either in a so-called electricity-driven or a heat-driven mode [2] [7]. The CHP plant considered here operates in a heat-driven mode, in which the primary goal is to satisfy the local heat demand. Nevertheless, the addition of a TES tank allows the plant operation to be decoupled from the heat demand, which opens up opportunities for improved operation strategies.

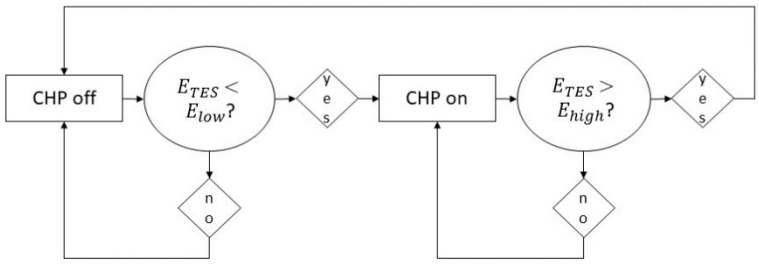

Figure 13: Decision tree illustrating the thermostat control logic.

2.6.1 Operation Strategies

A common operation strategy for heat-driven CHP plants equipped with TES systems is thermostat control [20]. Hereby, the TES' energy content (or temperature level) essentially serves as a decision

[4] The technical feasibility of syngas injection into the gas grid and the necessary purification steps are outside of the scope of this report. (See Outlook, Section 5)

variable. The CHP is switched on when the TES level drops below a fixed lower threshold and turned off again once the TES has been filled to reach an upper threshold.

Figure 13 illustrates the control logic in the form of a decision tree. This approach is used as a baseline.

In a second approach, the standard thermostat operation is modified to increase its flexibility and allow the CHP plant to be more self-sufficient in meeting the local electricity demand. For this purpose, a second set of thermostat thresholds is introduced that is used whenever current electricity demand levels result in economically favourable operating conditions. The updated control logic decision tree is shown in Figure 14. The second set of thresholds, which is used whenever the break-even point is reached (high electricity demands), can then be chosen to promote CHP operation during times when it is lucrative. Meanwhile, the regular thresholds can be adjusted to limit operation below the break-even point to the necessary minimum for ensuring heat demand coverage at all times. This new operation strategy is thus a hybrid of heat-led and electricity-led operation.

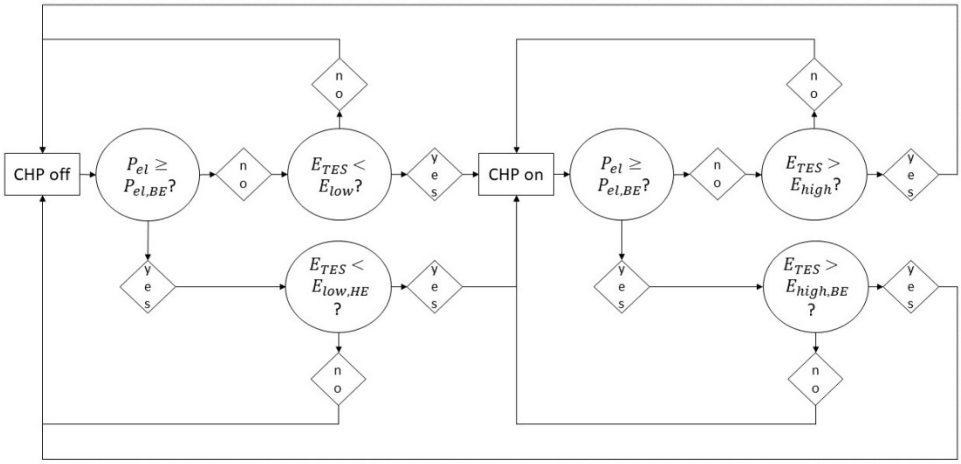

Figure 14: Decision tree illustrating the hybrid control logic.

The inclusion of a SMR into the CHP system requires an expansion of the operational control mechanism. As long as the engine is running and the exhaust temperature is sufficiently high (min. starting condition is 550 °C), the SMR can be switched on or off independently. To reap the maximum possible benefits from the SMR inclusion, however, the reformer is operated as much as possible. It is only switched off (i.e., bypassed) in case the heat-demand coverage becomes critical ($\dot{Q}_{dem} \geq \dot{Q}_{crit}$). Below this threshold, the CHP is guaranteed to be able to satisfy heat demand even with SMR operation. The steam reformer is also switched off whenever TES energy levels fall below the lower threshold, E_{low}.

2.6.2 Optimisation Procedure

The optimisation of the control parameters requires a large number of optimizations runs over the entire one-year timeframe, for which the detailed Simulink model is too computationally expensive. Instead, a very simple linear model (see Section 2.6.3) is used for finding optimal parameter values. The linear model is formatted as a Matlab-function that is called by a pattern-search optimiser to search for TES threshold parameter sets, which result in an optimal objective function. To this end, the pattern search can either be called with a genetic algorithm or latin hypercube search option, both of which are combined with the standard polling method of the generalized pattern search (GPS) algorithm (positive basis 2N). The results of an initial optimisation run using the latin hypercube search (with 1000 samples per parameter) serve as an initial guess for a second search using the genetic algorithm. The objective

function weights second law efficiency, degree of self-sufficiency, and operating costs equally (reference values are obtained from a perfect foresight optimisation using the Gurobi solver):

$$objFcn = \frac{1}{3} \cdot \left(\frac{DSS}{DSS_{ref}} + \frac{\varepsilon}{\varepsilon_{ref}} + \left(\frac{cost}{cost_{ref}} \right)^{-1} \right)$$ Equation 3

Due to the hourly resolution, there is a discrepancy between the operational behaviour defined by the thresholds and the actual behaviour of the linear model. To mirror the same optimal model behaviour exhibited by the linear model in the more detailed Simulink model (which makes dispatching decisions every second), threshold parameters have to be "translated". Identifying instances where the engine is switched on below the lower threshold and turned off above the upper threshold respectively and taking the median of these points as actual threshold parameters is found to lead to good agreement between the models.

2.6.3 Linear Model

The linear model is set up in cooperation with the LAV Energy Systems Group. It uses discrete time steps of one hour and is fundamentally based on two energy balances: An electrical energy balance (Equation 4) and a thermal energy balance (Equation 5):

$$P_{el,grid}(i) = P_{el,dem}(i) - u_{ICE}(i) \cdot P_{el,nom}(i)$$ Equation 4

$$E_{TES}(i+1) = E_{TES}(i) + \dot{Q}_{CHP}(i) - \dot{Q}_{dem}(i) - \dot{Q}_{TES,amb}(i)$$ Equation 5

where *i* represents the current time step; u_{ICE} is the CHP's on/off signal; $P_{el,grid}$ represents the electrical power exchanged with the electricity grid, where positive values indicate electricity being provided by the grid; $P_{el,nom}$ is the CHP's nominal electrical power output. The variables in Equation 5 are: E_{TES} is the TES system's state of charge (in kWh); $\dot{Q}_{CHP}$ is the hourly averaged thermal power output of the CHP; and $\dot{Q}_{TES,amb}$ represents the TES heat losses to the environment. The CHP's hourly averaged thermal power output is calculated according to Equation 6:

$$\dot{Q}_{CHP}(i) = u_{ICE}(i) \cdot P_{th,nom} - \Delta P_{th,start}(i)$$ Equation 6

where a thermal power deficit $\Delta P_{th,start}$ is subtracted from nominal power output in the first hour of operation (i.e., after every start) whose size depends on the duration of the preceding cool-down period[5].

If an SMR is added to the linear model, Equation 6 becomes

$$\dot{Q}_{CHP}(i) = u_{ICE}(i) \cdot P_{th,nom} - \Delta P_{th,start}(i) - u_{SMR}(i) \cdot \Delta P_{th,SMR}$$ Equation 7

[5] A maximum 30 % of the nominal power output is subtracted from the hourly averaged thermal power, if the engine has cooled off for at least six hours. For cool down intervals shorter than six hours, this start-up power deficit is linearly reduced.

where u_{SMR} is the SMR on/off signal and $\Delta P_{th,SMR}$ is the thermal power that is diverted and used in the SMR. The steam reformer's chemical output is calculated based on nominal hydrogen production rates. To account for steam reformer warm up, which is assumed to take around 30 minutes, the chemical output is halved for the first hour of SMR operation.

2.7 ReMaP Simulation Framework

The SFW is a simulation platform written and developed in python as part of ReMaP Task 3.8 at ETH's Research Centre for Energy Networks (FEN). It allows hardware from different locations (PSI, Empa, ETH, etc.) and software models to be connected with each other and a common data archive. It therefore enables flexible experiments ranging from pure simulation to hardware-in-the-loop (HIL) or even pure hardware tests from distributed remote locations. In the following, only functionality important for investigations of Task 3.5 will be discussed in detail.

2.7.1 Data Logging

Data of all components and models connected to the SFW or ReMaP platform is logged on a common data archive provided by the Venios platform. For the purpose of Task 3.5, this includes experimental CHP/SMR data, SFW simulation data and demand data from NEST (Section 2.7.5). Control and status signals, which are usually Boolean or integer, are logged when they change. Measurement values, which are usually floating-point values, are also logged when they change, but at least once every five minutes and at most once per second. These rules are implemented to reduce the load on the system and make it perform more robustly.

2.7.2 Linking the Laboratory Plant to the SFW and Data Logging Environment

A programmable logic controller (PLC) is the binding element between the local control of the machine (the ECU) and the SFW. The PLC transmits all measurement values from the plant to the SFW and all control commands from the SFW to the plant. The PLC is connected with the ECU via a CAN-bus and with the SFW via the internet. Once remote-control access is given, the control command coming from the controller running in the SFW is transmitted to the PLC and from there forwarded via CAN-bus to the ECU.

2.7.3 Adjustment of Existing Simulink Models for Application in the SFW

To include Simulink models into the SFW and enable HIL simulations, they need to fulfil one important requirement: They need to be executable in real-time. For the purpose of Task 3.5, this is achieved by including a "Real-Time Sync" Block (part of the Simulink desktop real-time toolbox) into the model. This ensures accurate simulation results in real-time, but also comes with two disadvantages: First, the Simulink desktop real-time toolbox is not included within the standard Matlab licence and can therefore be expensive to use, which may limit model availability for users of the SFW. Alternative implementations, like the "real-time pacer for Simulink" (available on the MathWorks file exchange), may mitigate the availability issues of Simulink models within the SFW. Secondly, this method only works reliably with a single Simulink model. To run multiple models in parallel, they have to be combined into one.

If a model fulfils this primary requirement, then all that is needed to connect it to the SFW is an initialisation function and a read/write function in Matlab. The former is called by the SFW code to load the model and initialize its parameters and initial conditions at the start of any simulation. The latter is called to handle model input/output at every time step. Both functions do not change drastically for different models and can thus easily be adapted for integration of new components.

2.7.4 Implementation of Controllers into the SFW

To integrate the CHP operation controller (described in Section 2.6.1) into the SFW, it is first translated from Matlab to the python programming language. It can then be included into the main SFW code as a custom class. Connection of the required feedback and control signals is then handled by the SFW itself.

2.7.5 SFW Demand Data

The SFW allows input of demand data from different sources at variable sample rates. Simulations can be run with user-supplied input files (i.e., hourly resolved demand data, described in Section 2.5.3); data stored in the Venios data archive or even live data available on the Venios platform. This allows HIL experiments to be conducted under the same conditions as the simulations described in Section 2.5 & 2.6 using the same demand data, but also offers the opportunity to use real-life and real-time demand data from Empa's NEST building. NEST is a modular building structure that is used for applied research in a number of semi-independent subunits, ranging from apartments to offices and a spa, among others. [3] Data from this building is also connected to the ReMaP platform and is stored in the Venios data archive. The demand data for individual subunits is logged at the interface to the building's core structure, six of which are available in the data archive. This allows the control strategies (described in Section 2.6.1) to be tested under realistic conditions. For this purpose, a series of experiments are conducted with demand data from three NEST units[6] lumped together (Section 3.5.3). These include a two bedroom and a three-bedroom apartment as well as a shared office space that is equipped with solar panels on its façade.

2.7.6 HIL Experiment Setup

Three combinations of physical and virtual components are used in HIL experiments via the SFW, the results of which are presented in Section 3.5. Figure 15 & Figure 16 show the setups for the first two HIL experiments (Section 3.5.1 & 3.5.2 respectively), which replicate the layouts used in long-term simulations (Section 2.5 & 3.3), replacing the CHP model with hardware and moving all other components (operation controller, TES model and hourly resolved demand data) into the SFW. The main purpose of these experiments is to test the SFW's HIL capabilities (including the performance of the adapted Simulink models) and to make sure the controller can handle hardware data. By using model-critical scenarios from the long-term simulations, the HIL experiments can also be used for further comparison of CHP model behaviour and hardware data[7].

[6] Unit Urban Mining & Recycling (two-bedroom apartment), Meet2Create (office space), Vision Wood (three-bedroom apartment).

[7] In addition to an in-depth validation of the model, which has preceded these experiments.

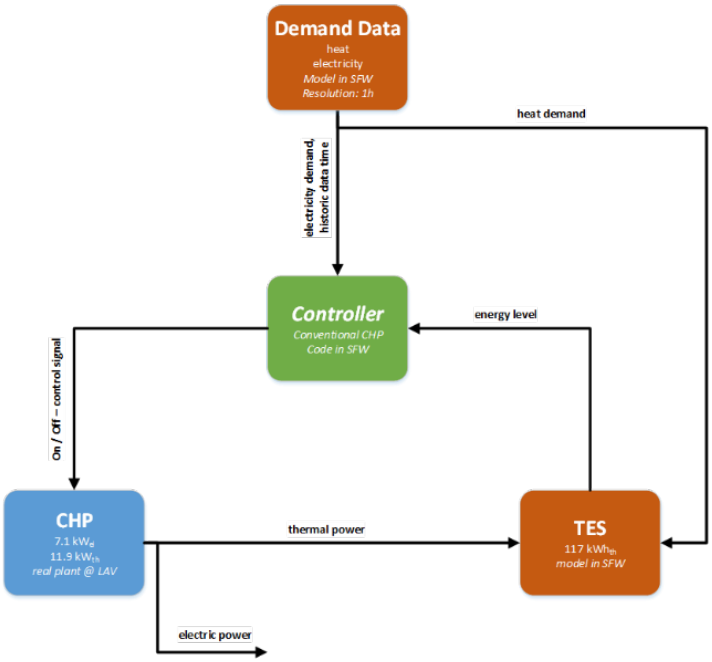

Figure 15: HIL layout 1: using CHP hardware along with hourly resolved demand data and TES model integrated in the SFW.

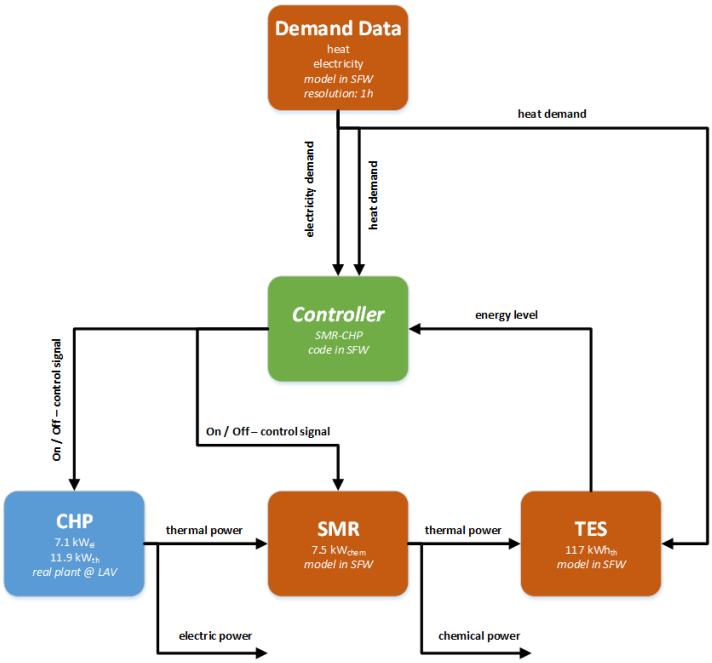

Figure 16: HIL layout 2: adding an SMR model (included in the SFW) to HIL layout 1.

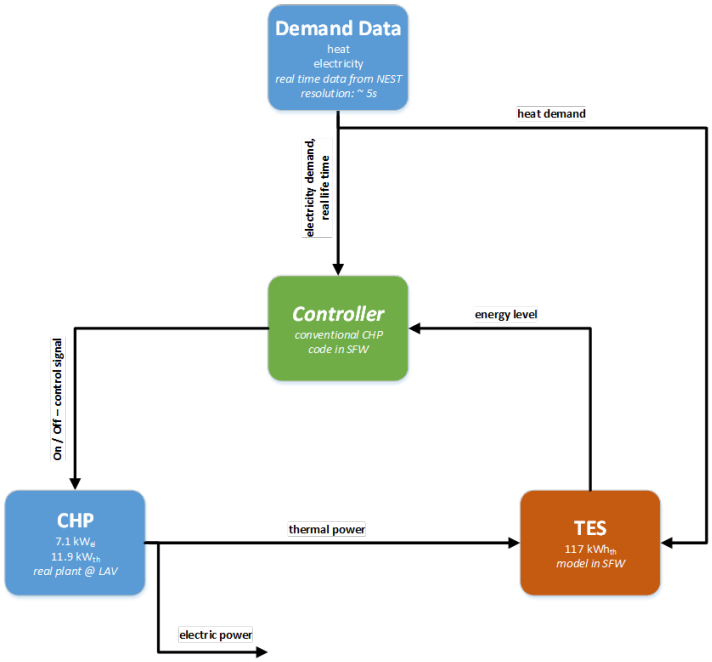

Figure 17: Layout for HIL tests with NEST demand data.

Figure 17 shows the setup for the third set of HIL experiments (Section 3.5.3). It is largely identical to the layout presented in Figure 15, with the important distinction of using NEST demand data, described in the previous section, rather than the hourly resolved demand data used for the long-term simulations. This allows the operation strategies to be tested under more realistic conditions, where the demand signals do not change on the hour but within a few minutes or seconds[8]. To be able to test and compare several different operation strategies and controller setups, the NEST demand is not used live but rather pre-recorded and reused for all tests. The controller, however, does not have any information of upcoming samples and thus performs as if the demand was a live input.

2.8 Evaluation of a Commercial mCHP Plant for NEST

The Aladin II CHP plant used in this report is a lab-scale prototype and therefore needs constant supervision. To expand the scope and duration of (HIL) experiments with CHP plants in the context of the future energy system, safe remote operation without direct supervision needs to be possible. Commercially available mCHP plants are hence evaluated for the use in a possible follow-up project that could move the concept into fields of more applied research. If possible, any replacement CHP plant should also retain the capability to retrofit an SMR. This section outlines the legal and technical requirements for such a replacement, while a selection of possible candidates is given in Section 3.6.

2.8.1 Legal Requirements

Commercial CHP plants installed in the canton of Zurich need to comply with emissions restrictions dictated by the ordinance on air pollution control (Luftreinhalte-Verordnung) [21]. For stationary gas-fired power plants with an output of less than 100 kW, it specifies a maximum of 650 mg/m^3 of carbon monoxide and 250 mg/m^3 of NOx emissions, measured at a 5% oxygen content. In addition, the canton of Zurich also mandates yearly emissions tests as well as complete and professional usage of the produced heat.

[8] The signals are recorded on change, but no faster than once per second and no slower than every five minutes.

According to the canton's office for emission control, these regulations can be relaxed somewhat for experimental installations. Nevertheless, it may make sense to work with hardware that fully complies with regulations and hence is viable on the commercial market.

2.8.2 Technical Requirements from NEST

At NEST, the new CHP plant would be integrated into a multi-energy system and coupled to an existing TES tank, which will mainly govern the CHP's operation (while not being used for special research tasks). The resulting technical requirements for the installation at NEST are not very restrictive and can be found in Table 4:

Table 4: Technical CHP requirements at NEST

Thermal Power	≈10 kW (or similar to Aladin II specs)
Electric Power	As high as possible
Installation Height	max. 2200 mm
Installation Floor Area	No restriction
CHP Outlet Temperature	min. 65°C

2.8.3 Additional Requirements for SMR Retrofit

If the possibility to retrofit the commercial CHP plant with a new SMR prototype is to be incorporated in this assessment, a few additional requirements have to be met. Namely, the replacement CHP should also be natural gas-fired to simplify logistics. It should further be operated at a stoichiometric air-fuel ratio and without turbochargers or Miller/Atkinson valve timing to supply the SMR with suitably high exhaust temperatures. The use of a multi-cylinder engine would further reduce the mechanical stress on the SMR reactor (compare to Section 3.2.2).

3 Results and Discussion

3.1 Fundamental Investigations Regarding SMR / BHE (Choice of Concepts)

To investigate the option of storing thermal energy in the ground, the existing borehole at Empa is modelled using the finite-volume model described in Section 2.3.1. Figure 18 shows the simulation results of the soil's storage capability for three loading durations. The ratio $(Q_{in}-Q_{out})/Q_{in}$ is a measure of the injected thermal energy share that is contained within a soil cylinder with a 5 m radius around the borehole. Where Q_{in} represents the thermal energy that is delivered to the borehole at 80°C within t_{charge} and Q_{out} is the thermal energy that has passed the boundaries of the control volume.

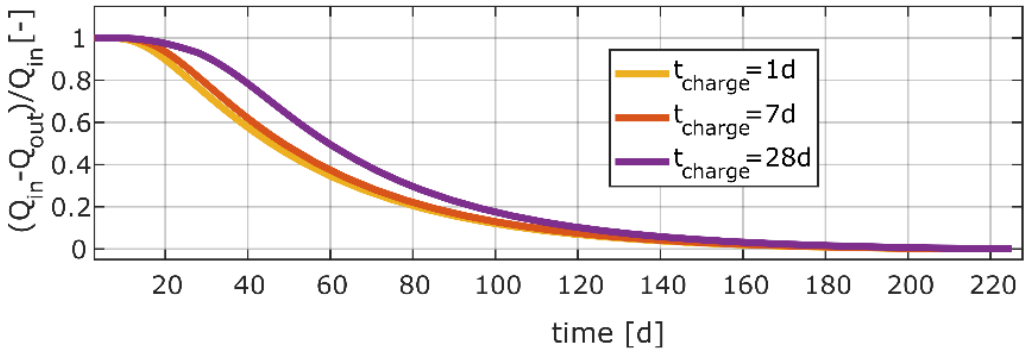

Figure 18: Thermal diffusion within a soil cylinder of 5 m radius around a borehole as a function of the charging duration in days, simulated using a validated finite-volume model.

The injected thermal energy diffuses out of the control volume completely within roughly 200 days regardless of the injected amount. After 50 to 60 days, already half of the injected thermal energy is lost. Only a share—depending on the waiting time—of the remaining thermal energy contained within the control volume can be effectively extracted due to the low temperature gradients in the soil. A single borehole is therefore not appropriate for seasonally storing thermal energy in the ground. Only insulation or a borehole field could improve the storage capability. However, these are expensive measures and it is therefore not economically feasible to combine borehole thermal storage with CHP plants on the investigated scale. [10] [22] [23]

The steady-state exergy analysis of a CHP process is conducted by calculating the exergy rates at the system inlet and outlet for two ideal systems, resulting in the exergy efficiencies shown in Figure 19. The available Aladin II CHP plant is taken as a reference for the CHP exergy calculations. While in the conventional CHP plant, all of the input exergy is transferred to the plant itself, in the SMR-CHP plant the input is split between the reformer (37%) and the CHP plant (63%). The output exergy splits into electrical and thermal exergy for both plants, plus chemical exergy for the SMR-CHP plant. The exergy efficiency of the SMR-CHP plant is 1.5 times higher than that of the conventional CHP plant, when also considering methane that passes through the SMR without reacting. The chemical energy recovered from thermal energy consists of H_2 (58%vol), CH_4 (27%vol) and CO (1%vol) (plus 14%vol CO_2) and can be used directly in another process or stored seasonally for example in the gas grid, depending on future development of the regulations for the gas grid.

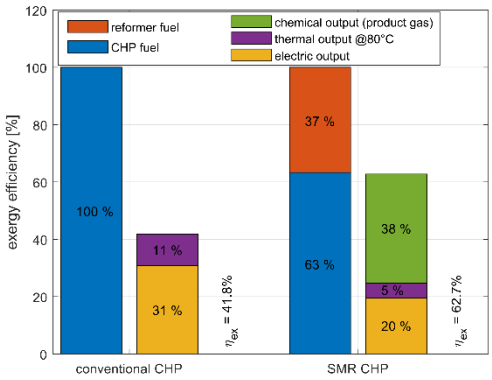

Figure 19: Steady-state exergy efficiency for the conventional (based on measurements) and SMR-CHP plant (based on SMR conversion efficiencies provided by the manufacturer).

From the results presented above, Concept 2 (see Figure 1) is concluded to be more promising. Therefore, it is decided to build an SMR-CHP test rig and investigate this option more deeply and with regard to applicability in practice. All following investigations are based on this decision and only consider Concept 2.

3.2 SMR-CHP Prototype Plant

3.2.1 Operation of the SMR

The SMR system could only be operated for a total of roughly 10 hours before an internal leak inside the reformer heat exchanger prevented the process from functioning. During these 10 hours of operation, 17 trial runs were performed but the composition analysis of the syngas was only available for the last four runs. By then, the system was already partially damaged. Therefore, no useful data about the chemical performance is available nor could a chemical steady state be observed.

The first 13 trial runs were commissioning runs, where the control system was tested and adjusted for a safe and robust operation. The main improvement was an automatic and adjustable prefill cycle with demineralized water for repeatable start conditions. In addition, all warning and error margins were set and the gas chromatographer for the composition analysis was adjusted and calibrated for this type of gas.

During commissioning, it turned out that the hysteresis controller is not suitable for the system. The abrupt pressure changes due to the cycling of FS-405 (see P&ID in Appendix 8.2) on the syngas side (see Figure 20, left) during transients causes flow oscillations through the heat exchangers, which again cause temperature oscillations (see Figure 20, right). Oscillating temperatures most probably influence the chemical conversion process in the reformer. In Figure 20, after 35 minutes the syngas mass flow is large enough to hold the pressure in the system and the cycling of FS-405 stops. At the same time, all temperatures also stop oscillating. A mechanical pre-pressure regulator will resolve this issue and most probably lead to a quicker establishment of stable chemical reactions. Another measure to reach a thermal and chemical steady state more quickly is to operate the system on pure water during the warm-up. Only once reformer temperature TI-401 is high enough, methane should be added to the process. This will also minimize chemical losses.

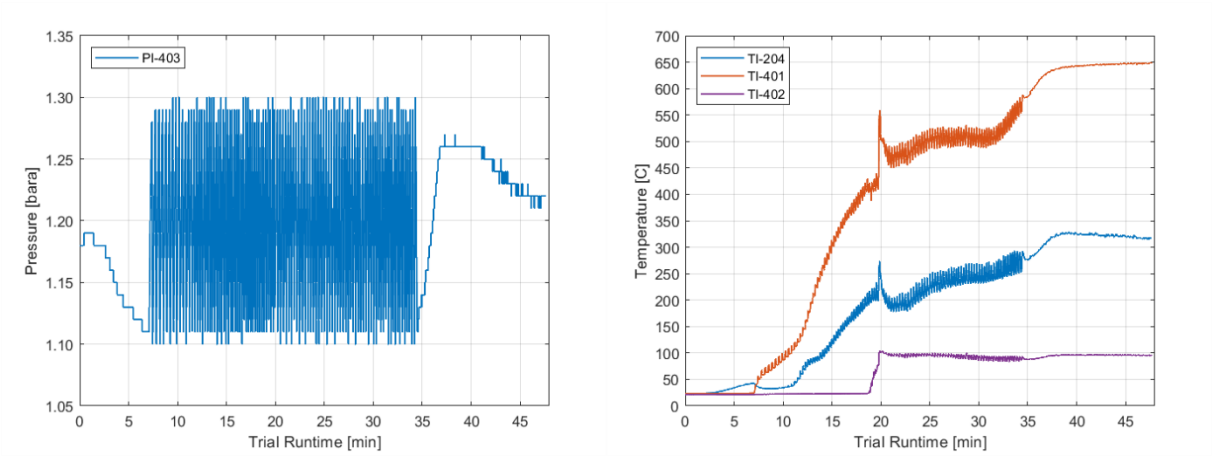

Figure 20: Syngas pressure (left) and three process temperatures (right) during a cold start of the SMR.

The next set of experiments were planned to serve as characterization runs, where the CHP was supposed to run in steady state to test varying flowrates and steam to fuel ratios. During the first of these experiments, an unexpected behaviour of the system was observed;

1. No chemical steady state was detected by the gas chromatographer even though the system was thermally stable and the mass flows did not change for more than 40 minutes (see Figure 21).
2. The nitrogen concentration increased towards the end of the experiment.

The non-steady chemical composition might have been caused by the oscillation problematic described above; the total mass flow for the first sweep test was so small, that the pressure was not steady yet and FS-405 was constantly opening and closing which caused massive local mass-flow fluctuations (e.g., inside the reformer). The high nitrogen concentration in the beginning of the experiment is normal, as there might have been venting air in the system before the experiment had started. The increase of the nitrogen concentration towards the end of the experiment is, however, suspicious. This anomaly prompted a closer examination of its cause.

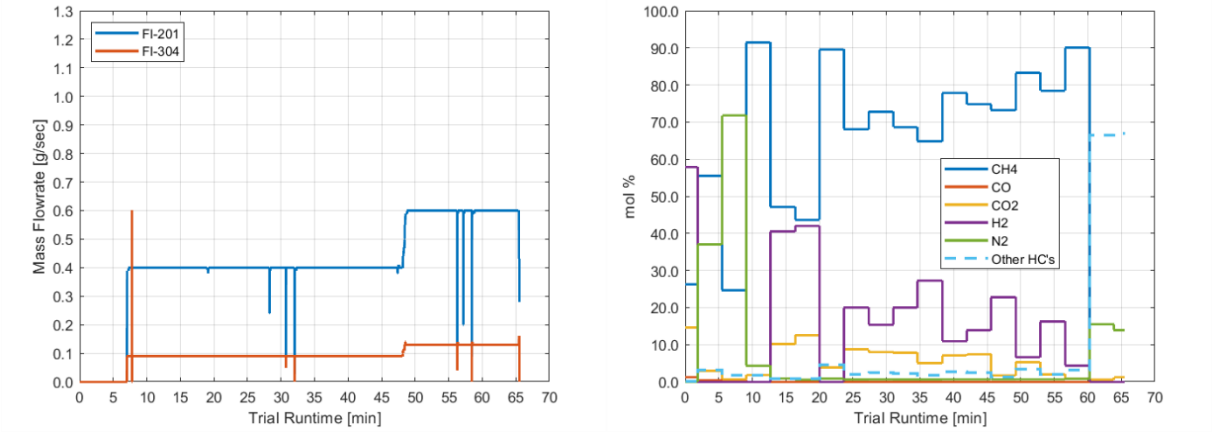

Figure 21: First mass flow sweep test. In the left graph, the mass flow for water (FI-201) and methane (FI-304) is shown. On the right side, the molar fractions of all components in the syngas are shown for the same experiment.

3.2.2 Failure Analysis

The first observation was that the syngas system could not hold pressure after the initialization cycle was completed. Figure 22 (left) shows the pressure traces for three different runs. During initialization, the pressure is increased by filling the system at 0.4 g/s of methane until it reaches 1.2 bar. A slight decrease over time as in the orange case, labelled “normal initialization” is no problem. The violet trace already shows a very fast pressure decay while in the green trace, the pressure did not rise above 1 bar absolute. The three pressure traces stem from three different days and show the increase in leak size. The leak was located inside the reformer heat exchanger E-101 (see P&ID in Appendix 8.2 and Figure 7). The leakage flow was finally quantified with 0.4 g/s methane at a pressure difference of roughly 3 mbar.

The heat exchanger manufacturer Bosal was contacted to identify the cause of the failure. Neither the temperatures nor the absolute pressure inside the heat exchanger ever exceeded design limits. Even though Bosal initially claimed that the exhaust gas pulsations (see Figure 22, right) would not affect the mechanical integrity of their components, they now said that these pulsations in combination with the very high temperatures E-101 is facing were most probably the cause of the failure. Bosal suggested to get rid of the exhaust gas pulsations before replacing the heat exchanger and proceeding with the experiments. Due to the long delivery time of the reformer of roughly three months, such a procedure was not possible within the temporal scope of this task.

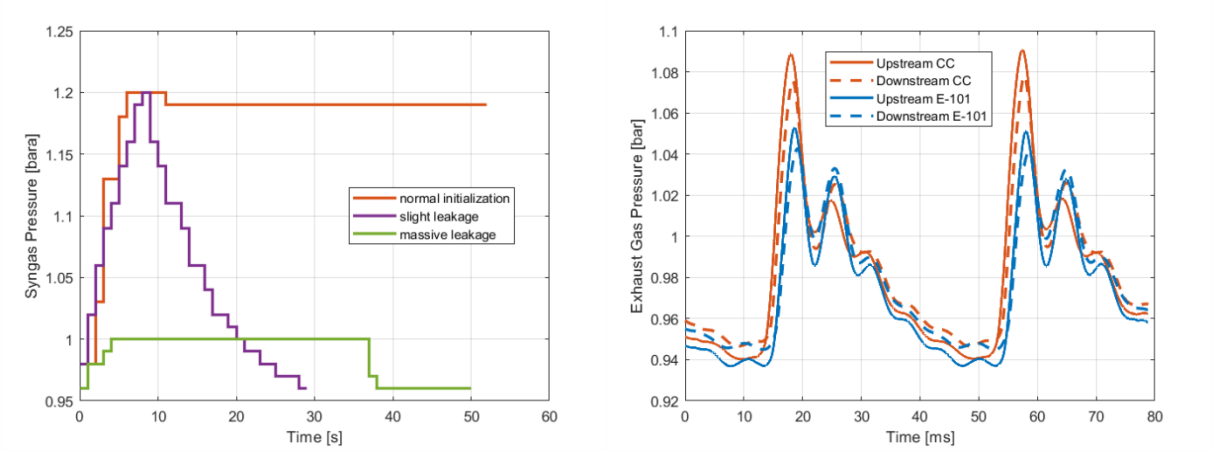

Figure 22: Pressure traces of the syngas during initialization (left) and pressure traces of the exhaust gas inside and outside E-101 (right).

3.3 Quantifying Improvements of SMR-CHP over Conventional CHP

The SMR-CHP is compared to the conventional CHP based on results using the improved hybrid operation strategy with optimised TES thresholds. Key results of simulations over an entire year are compared in Table 5 for configurations with and without SMR. The table indicates overall positive results for the SMR-CHP configuration: Total CHP runtime is up by 39.4 % while the SMR can be used for more than two thirds of the time. The increased running hours have a positive impact on the degree of self-sufficiency, which has gone up by 30.7 %. In combination with a decrease of starts, the extended runtime also caused the average continuous operating hours to go up. This reduces the plant’s thermal power losses through transient operation, which, in conjunction with the SMR’s hydrogen production, led to an exergy efficiency increase of 8.6 %[9]. The SMR’s impact is not positive in all respects, however, as the SMR-CHP’s running costs have gone up by 15 % relative to the base CHP configuration.

[9] When only considering the additional chemical energy converted from exhaust enthalpy but not the methane feedthrough.

Table 5: Key results comparison SMR-CHP and conventional CHP

Parameter	*Conventional CHP*	*SMR-CHP*	*Unit*	*Delta*
CHP Runtime	3005	4188	h	39.4%
SMR Runtime		2852	h	
CHP Starts	381	366	-	-3.9%
Median Runtime	4.8	4.9	h	2%
2nd Law Efficiency[9]	33.7	36.6	%	8.6%
DSS	45.6	59.6	%	30.7%
Electricity Export	69.7	71.6	%	2.7%
Operating Cost	7391	8507	CHF	15.1%

Figure 23 presents a closer look at the SMR-CHP operation throughout the year. The upper plot shows an increase in runtime for the SMR-CHP compared to the conventional layout over the whole simulation period. The middle plot shows an increase in the number of starts in summer, compared to the conventional CHP, when the SMR-CHP's reduced heat-to-power ratio allows it to be operated more often and catch more electricity demand peaks. The bottom plot shows how the SMR usability is limited by large heat demand in winter. It, however, presents an additional degree of freedom, allowing thermal power to be adjusted according to demand while providing full electrical power and maintaining high exergy efficiency without having to power-cycle the CHP. This flexibility is based on the assumption, that the SMR can be switched off independently of the CHP and can effectively be bypassed. Such a bypass would also need to be integrated in a next iteration of the SMR prototype.

The degree of self-sufficiency, shown in Figure 24 (top plot) reinforces previous findings by displaying DSS values for the SMR-CHP, which are always higher than values for the conventional CHP, with the most extreme relative differences occurring in summer. Meanwhile, the bottom plot shows that there is no dramatic increase in the percentage of produced electricity that has to be exported to the grid. This means, the additional electricity production of the SMR-CHP can still be effectively used to cover local demand instead of having to be offloaded to the grid.

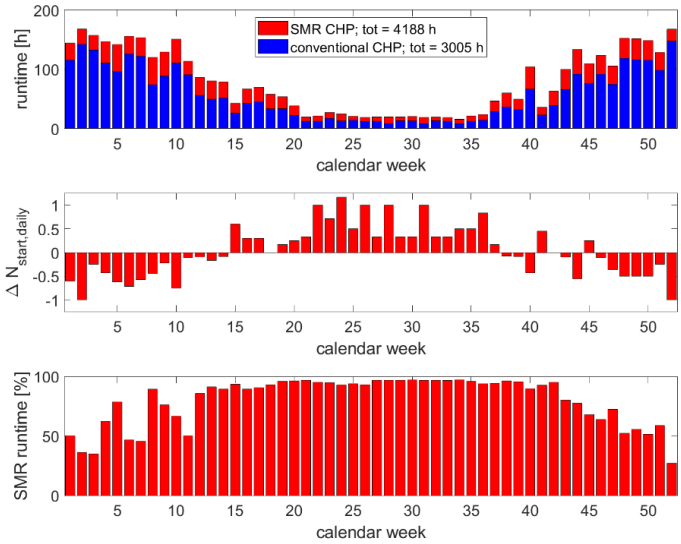

Figure 23: SMR operation characteristics. Impact on CHP runtime (top) compared to conventional CHP runtime. Difference in daily number of starts, averaged per week (middle). SMR runtime as percentage of SMR-CHP operation (bottom).

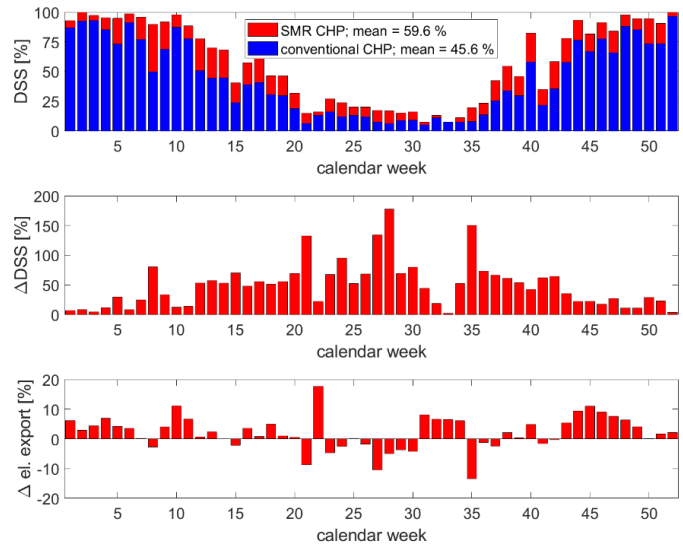

Figure 24: Comparison of CHP electricity balance with and without SMR: The top plot shows the degree of self-sufficiency, the middle plot shows the relative difference in DSS $\left(\Delta DSS = \frac{DSS_{SMR} - DSS_{conv}}{DSS_{conv}}\right)$ and the bottom plot illustrates the relative difference in exported electricity (relative to electricity production) with and without SMR.

Figure 25 gives an overview of the electricity import (top) and export (middle) for both configurations as well as the SMR's production of chemical energy (bottom). For both configurations, electricity imports mainly occur during summer, while exports are largest during winter months. In this respect, CHP behaviour is very much complementary to renewable electricity production, in particular solar PV. The differences between SMR-CHP and conventional CHP are a direct function of runtime and degree of

self-sufficiency discussed before. It should be noted that 1.4 MWh of the 5.1 MWh additionally produced chemical energy (syngas) coincide with calendar weeks 14-39 (roughly April to September). The remainder (ca. 73%) is produced during winter months (ca. October to March). To put this into context, the conventional CHP consumes 69.5 MWh (LHV) of natural gas during its 3005 hours of operation.

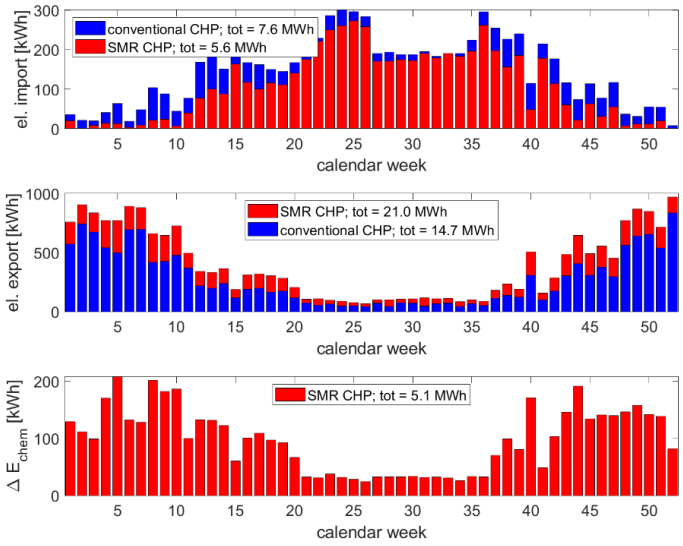

Figure 25: Comparison of electricity import (top) and export (middle) for the SMR and conventional CHP as well as production of additional chemical energy (bottom).

3.4 Operation Strategy

In this section, results obtained by applying a novel hybrid control strategy (introduced in Section 2.6) are compared against standard thermostat control. The principal goal of the new operation strategy is the improvement of the system's DSS and therefore its operational flexibility without jeopardizing heat demand coverage or sacrificing efficiency. Table 6 presents the optimised TES thresholds for all combinations as well as the additional, SMR-related, demand threshold (Q_{crit}). TES thresholds are given as a percentage of maximum tank capacity.

Table 6: Optimised thresholds for all combinations of configurations and operation

	Conventional CHP		*SMR-CHP*		*Units*
Strategy	Thermostat	Hybrid	Thermostat	Hybrid	
E_{low}	55.85	49.97	64.19	54.85	%
E_{high}	93.11	86.87	89.56	78.66	%
$E_{low,BE}$		77.42		77.92	%
$E_{high,BE}$		91.38		90.80	%
Q_{crit}			6775	6775	W

While the standard thermostat control yields a minimal runtime of 4.2 h (compared to 1.25 h for hybrid control), the hybrid control approach shifts a significant share of operation into the range of one to four

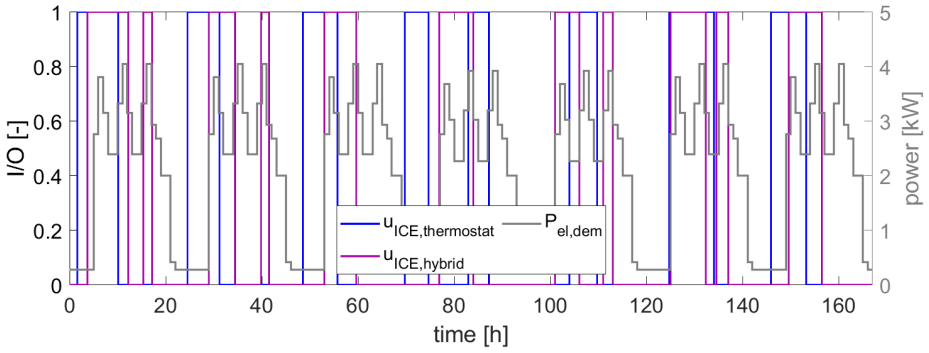

Figure 26: Operating pattern of hybrid (purple) and thermostat (blue) approaches for a typical spring week (week 12) along with electricity demand (grey). All results concern the conventional CHP layout.

hours (almost 40% of all runs). A large share of these starts is initiated because the break-even point is surpassed. For instances of longer continuous operation, the two strategies do not differ drastically. The dispatching behaviour for both strategies is illustrated in Figure 26 for a typical spring week. With hybrid control, the CHP operation is better synchronised to electricity demand, exclusively running during the day and catching at least two of the three daily demand peaks. Thermostat control lacks this synchronisation and therefore also dispatches the CHP at night.

Figure 27 gives an in-depth look at the strategies' impacts on the electricity balance. The hybrid approach leads to an increase in total electricity coverage from 41.8 % to 45.6 %. This increase manifests itself throughout most of the year, with only a few weeks showing minor decreases of up to −3 %. These coincide with times when electricity demand rarely or never reaches the break-even point and the hybrid strategy hence loses its effectiveness. The largest relative increases in degree of self-sufficiency coincide with the transitional seasons and with periods of high electricity demand in summer. Simultaneously, the hybrid approach shows a reduction in the fraction of exported electricity that mostly mirrors the trends observed for changes in DSS. During winter, continuous operating times are long enough that many electricity demand peaks are covered regardless of specifically targeted operation.

The combination of increased DSS and reduced electricity exports at constant CHP runtime is a clear indication of smarter and more flexible CHP dispatching.

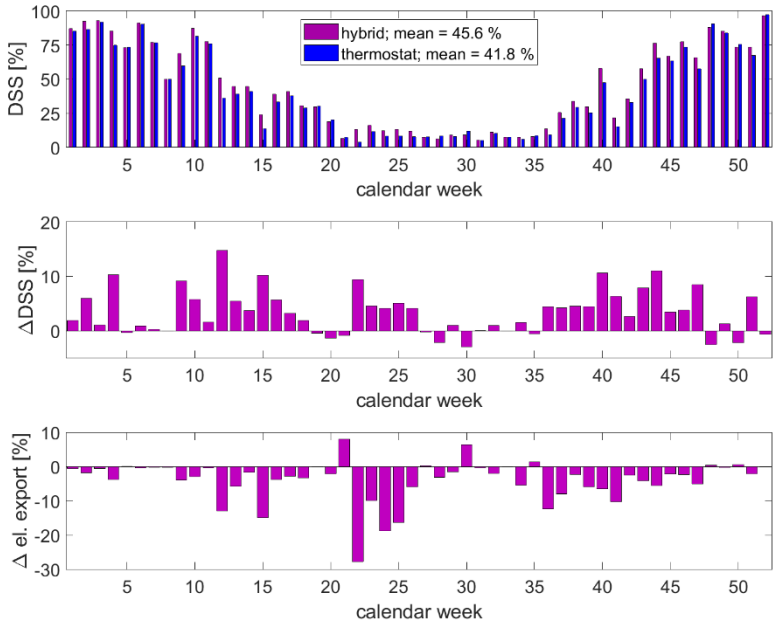

Figure 27: Comparison of degree of self-sufficiency (top), change in DSS relative to thermostat control (middle) and change in electricity export fractions relative to thermostat control (bottom) for thermostat (blue) and hybrid (purple) approaches. All results obtained for the conventional CHP configuration.

Table 7 gives an overview of key results. The hybrid approach strikes a good balance between cost and reward, increasing the DSS by 9.1% and reducing electricity exports and costs by 3.6% and 1.9% respectively. These improvements are paid for with an additional 87 starts (+33 %) and a decrease in second law efficiency of 0.2 percentage points (−0.6 %).

Table 7: Key results for both strategies (conventional CHP only)

Parameter	*Thermostat*	*Hybrid*	*Unit*	*Delta*
CHP Runtime	3007	3005	h	-0.1%
CHP Starts	294	381	-	29.6%
Median Runtime	7.2	4.8	h	-33.3%
ε	33.9	33.7	%	-0.6%
DSS	41.8	45.6	%	9.1%
Electricity Export	72.3	69.7	%	-3.6%
Operating Cost	7533	7391	CHF	-1.9%

3.5 HIL Experiments with the ReMaP Simulation Framework

Further information about the setup and motivation for the experiments presented in this section can be found in Section 2.7.6.

3.5.1 Conventional CHP: Comparison to Simulation Results

The experiments presented in this section are used to confirm agreement between experimental prototype and simulation data and to test the functionality of the SFW (converted Simulink models and overall HIL capability). The scenarios used for these experiments (and the one described in Section 3.5.2) are based on excerpts from the full year-long simulations of Section 3.3.

In a first HIL experiment, the SFW setup is used to compare CHP prototype behaviour with the Simulink model described in Section 2.2 using a relatively short operation interval, where the CHP is started from completely cold conditions. The start is initiated due to economically favourable conditions following an increased electricity demand from 07:00 A.M. This tests the control loop via the SFW and the performance of the TES level in its real-time, SFW-integrated form.

Figure 28 illustrates the results of this experiment. Overall, there is good agreement between simulation and experimental data. However, two areas of divergence can be observed. Firstly, the model slightly over predicts the thermal power output during the later stages of the transient start-up (between ca. 07:15-07:30) which is one of the most difficult parts to model. Secondly, the CHP is switched off with a delay of almost four minutes compared to the simulation. This is in part caused by the former divergence and in part by a steady state thermal power difference of around 200 W. Both of these factors cause the higher TES level threshold to be reached later during the HIL experiment and hence delay the shutdown of the plant. Around 50% of the resulting delay can be accredited to either cause. The steady state offset is in part due to the day-to-day variation in environmental conditions, which are not taken into account in the model, and in part to the performance degradation of the CHP's thermal insulation.

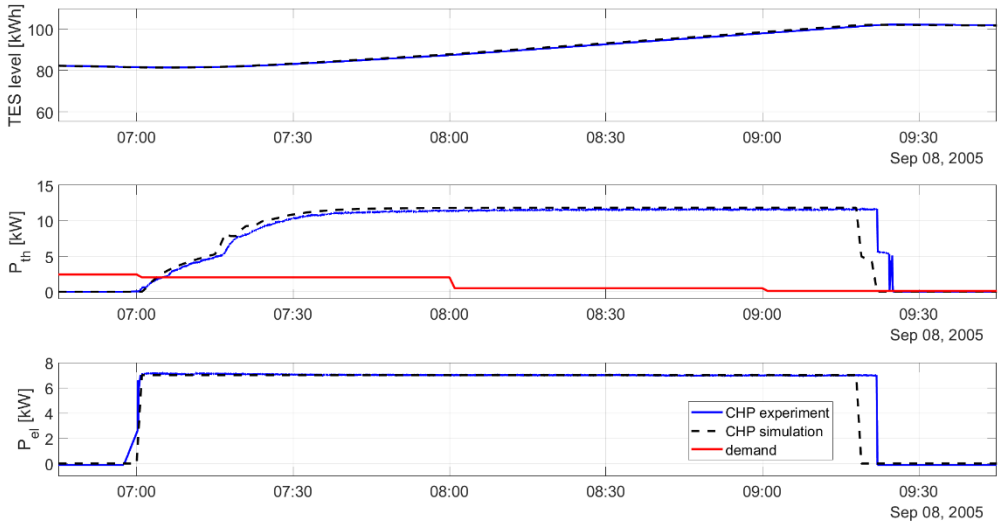

Figure 28: Results of the first HIL experiment. Top plot: TES level over time. Middle: Thermal power output as well as heat demand (red). Bottom: Electrical power output. Simulation results are depicted with black dotted lines while HIL results are displayed in blue.

For the second HIL test, the CHP was operating at steady state conditions until just before the start of the experiment and then rests until 7 A.M., when a high electricity demand prompts it to be switched on again. This tests the CHP model's capability to predict transient behaviour from various thermal states of the system. Results can be seen in Figure 29.

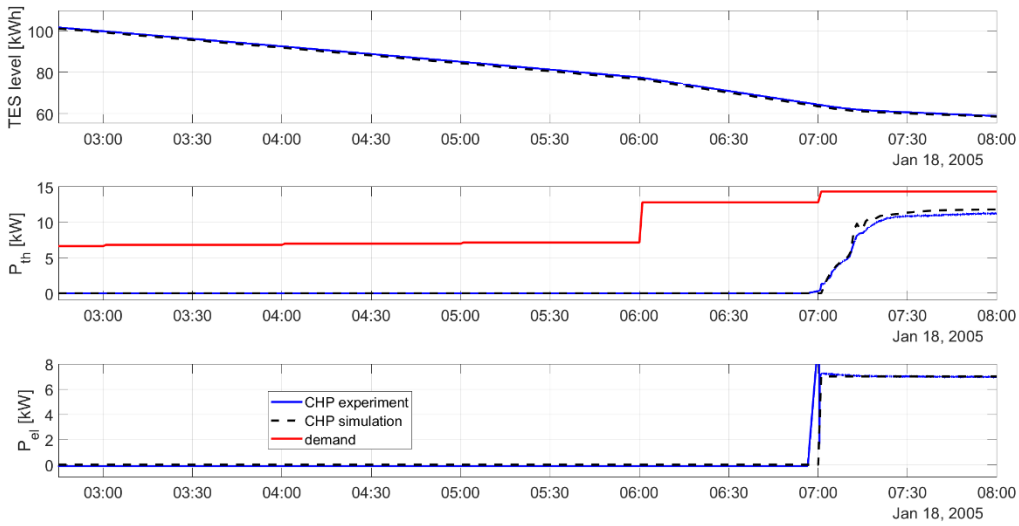

Figure 29: Results of the second HIL experiment. Top plot: TES level over time. Middle: Thermal power output as well as heat demand (red). Bottom: Electrical power output. Simulation results are depicted with black dotted lines while HIL results are displayed in blue.

The initial ramp-up of thermal power matches very well between model and hardware, while the later transient phase is somewhat overestimated in the model. On its way to fully steady-state operation, there is also a gap between simulation and experiment, which is due in large parts to a degradation of the CHP plant's thermal insulation, which has changed since the model was validated. During this experiment, the maximum thermal power output was as low as 11.3 kW compared to the modelled 11.8 kW. The large spike in electrical power (top plot, blue line) when the CHP is started shows the generator power that is used to crank the engine up to its operating speed. The generator power does not ramp up as early as suggested by the graph since the last data point before the peak is a couple of minutes older and the line connects them linearly.

3.5.2 SMR-CHP: Comparison to Simulation Results

This particular excerpt of the one-year simulation is chosen because it demonstrates a lot of the SMR control logic and operation. Before comparing experimental data to simulation data, an explanation of the chronological events shall be given. For now, only the dotted lines in Figure 30, representing simulation data, are of interest. The experiment starts with the CHP in standby mode. At 05:04 A.M, the TES level (top plot) reaches its lower threshold, which causes the CHP to be switched on (bottom plot, dotted line). Initially, thermal power is exclusively delivered to the heat storage tank until the lower threshold is surpassed again at 05:21 A.M. At this point, the CHP has warmed up sufficiently to start operating the SMR and because the heat supply is now no longer critical, the SMR is started (bottom plot, green dotted line). At 6 A.M., the heat demand increases and exceeds the CHP's thermal power output, causing the TES to be depleted again until 06:50 A.M. when the level drops below the threshold. To secure heat demand coverage, the SMR is hence switched off again making full thermal power available.

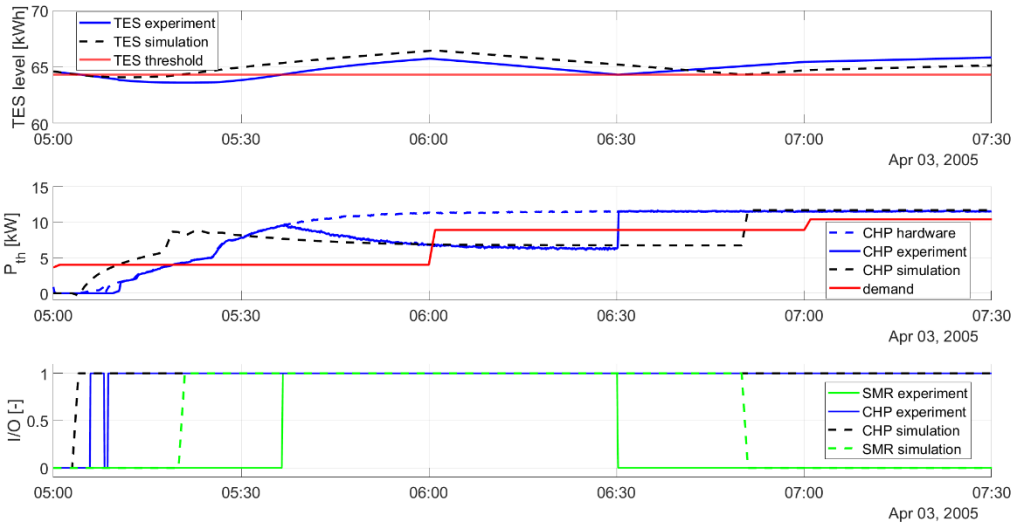

Figure 30: Results of the SMR HIL experiment. Top plot: TES level over time for experiment (blue) and simulation (black dotted) with lower TES threshold (red). Middle: Thermal power output for simulation (black dotted), CHP hardware signal (blue dotted), experiment including SMR model (blue) and heat demand (red). Bottom: Control commands (1 = on, 0 = off) for the CHP in black/blue and the SMR in green.

As can be seen from the solid blue and green lines in Figure 30, the experimental behaviour deviates from what is described above. This deviation is caused by a delayed start of the CHP due to communication problems[10] (visible by looking at the difference in CHP hardware and CHP experiment (SFW) thermal output signals in initial stages (05:05-05:10), when they should be identical). This leads to a lower TES level, which in turn delays the SMR start (only possible once TES threshold (top, red) is crossed) from 05:21 to 05:36 A.M. Since the experimental behaviour starts to match the simulation after the SMR is finally started, there is no way for the TES level deficiency to be made up. Consequently, the lower TES threshold is reached again sooner (at 06:30 A.M.), causing the SMR to be switched off earlier.

Apart from this unfortunate initial communication problem, the HIL experiment ran smoothly and followed the desired dispatching rules correctly. During times when both HIL experiment and simulation operate in the same mode, their behaviour matches reasonably well.

3.5.3 Operation Strategy Test with NEST Demand Data

This setup (described in Section 2.7.6) is used to test how well the hybrid operating strategy can cope with live demand data, which is sampled on change. The red line in Figure 31 shows the performance tested in a pure Simulink simulation (dotted) and in the HIL experiment (solid line). As can be seen, the CHP is switched on when a very short peak in electricity demand is reached. The CHP continues running afterwards, because the strategy is set up to avoid very short operation intervals, during which very little thermal power would be delivered. In this particular case, the CHP still runs long enough to also catch the larger demand peak at around 21:00, but there might not always be a larger peak following closely enough for this switch-on behaviour to make sense.

To address this, a moving average filter is introduced for electricity demand signals. The sliding window range of ten minutes is chosen to ensure the filter reads at least two samples and is large enough to ignore demand peaks that are unpractically short. The results of using this filter are represented with

[10] Between 05:02:21 and 05:10:30, the simulation was only able to complete four steps, producing four data samples.

green lines in Figure 31. Both during pure simulation and HIL experiments, the CHP is switched on a couple of minutes after the start of the large demand peak, covering most of the high electricity demand.

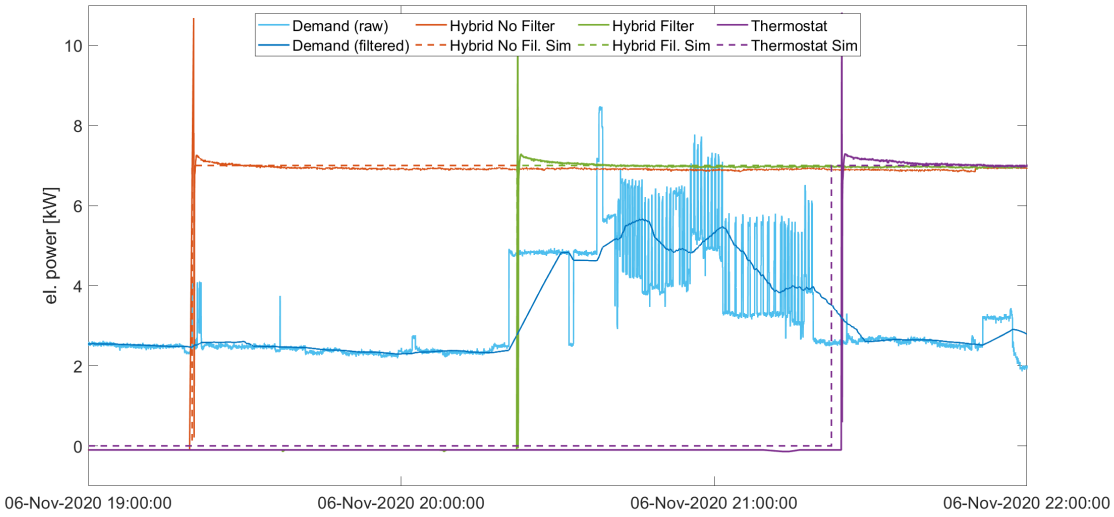

Figure 31: HIL experiment using NEST demand data. Light blue: unfiltered demand; dark blue: filtered demand (moving average, 600 s); red: hybrid strategy, no filter; green: hybrid strategy with filter; purple; thermostat strategy (w/o filter).

For further comparison, the purple lines illustrate the performance of the thermostat control strategy. It only starts the CHP once the demand peak is already over. In this case, the start is initiated because the TES reaches its minimal energy level. The mismatch between CHP starts in the experiment and simulation for this case has two causes: First, there is a 25-second delay between when the TES threshold is reached and when the CHP receives the command to switch on. This is within the general experience with early versions of the SFW and Venios data archive software. And secondly, when the simulation reaches the TES threshold, the experimental value is offset by 200 Wh, causing it to reach the threshold 89 seconds later. That offset could be caused by short transmission interruptions or slow connections, during which the latest heat demand signals did not reach the TES model in the loop. Otherwise, the HIL experiment results are in good agreement with simulation data.

3.6 Commercial CHP Plants for Potential Integration in NEST

A list of commercially available micro-CHP plants is printed in Table 8. All of the listed CHP plants meet the local emissions regulations and are comparable in size to the Aladin II prototype and the requirements presented by NEST. Based on the available manufacturer information, none of the presented systems have trouble meeting the NEST requirements regarding CHP outlet temperature and installation height (Section 2.8). A couple of micro-CHPs, which are considered to be particularly suited, are highlighted in the following.

3.6.1 KW-Energie Smartblock 7.5

Produced by KW-Energie in Germany, the Smartblock 7.5 mCHP is notable for very high overall efficiency and low emissions. It is available on the Swiss market via a local distributor[11]. This option had previously been assessed during the Aladin II project and the integration of a steam reformer has been discussed with the manufacturer. Latest iterations of the plant are being advertised as "H_2 ready" (i.e.,

[11] 42technology AG (Ltd.), www.42technology.ch

the CHP can handle up to 40% of hydrogen in the fuel) meaning SMR products could potentially be recirculated to the engine. These two points would make the Smartblock particularly well suited as a basis for continued investigations of SMR-CHPs.

3.6.2 EC-Power XRGI 9

The XRGI 9 m-CHP features very low emissions and a high electrical efficiency allowing it to meet all requirements for an installation at NEST and an SMR upgrade. It is also offered in Switzerland through a local distributor[12] from which a comprehensive quotation is available. Unlike the Smartblock CHP, the topic of an SMR upgrade has not yet been discussed with the manufacturer nor the supplier of the XRGI 9 CHP.

[12] BES BHKW Energie-Service AG, www.bes-ag.com

Table 8: Selection of commercially available mCHP plants comparable in size to the Aladin II prototype. Adapted from Schürch et. al. [4]

Model / Manufacturer	**Engine**			**P_{el} [kW]**	**P_{th} [kW]**	**Efficiency [%]**			**Emissions [mg/m³] at 5% O_2**	
	Cylinders	Displacement [cm³]	Speed [min⁻¹]			electric	thermal	total	CO	NO_x
Aladin II	1	325	3000	7	11.8	30.3	51.1	81.4	30.5	12.5[13]
neoTower 7.2 / RMB Energie GmbH	3	1000	1550	modul. - 7.2	modul. - 18.1	31.2	78.3	109.5	N/A	N/A.
Smartblock 7.5 / KW-Energie	3	972	1500	7.5	22.9	26.8	81.8	108.6	36.6	79.2
Energator GB 7.5 / Giese Energie	3	996	1500	modul. - 7.5	15 / 18.6	27.37	67.88	95.26	< 150	< 125
Vitobloc 200 EM-6 / Viessmann	3	952	1500	6	14.9	27	67	94	< 300	< 250
GTK 7 / Wolf Power Systems	3	972	1540	7	18	24.1	62.1	86.1	< 150	< 125
Muscetier NG 10 / ETZ GmbH & Co KG	3	1000	1500	modul. - 7.5	modul. - 19.6	30.7	58.6 / 72.5	89.3 / 103.2	120	20
XRGI 9 / EC Power	3	953	1500	9	19.2 / 21.3	30.6	64.9 / 72.7	95.5 / 103.3	55	54
Totem 10 / TOTEM Energy s.r.l.	4	1368	1500	modul. - 10	modul. - 23.6	30	67	97	< 10	< 10
6TO / Indop	3	953	1500	6	13.9	28.2	65.3	93.5	70	85

[13] Emission values (CO and NO_x) for slightly different configuration of the Aladin II prototype [4] [1]

4 Conclusions

The combination of CHP and BHE increases flexibility almost infinitely but simulations show that due to high heat-diffusion rates occurring based on the axis symmetry of the problem, it is not efficient to inject the produced heat into the ground at 80°C. Other thermal storage options may yield better results, a TES buffer tank, for example is an invaluable addition to any mCHP system. Combining the CHP with an SMR process on the other hand, increases both flexibility and exergy efficiency at once. This system compared to the conventional CHP set-up increases the degree of self-sufficiency (DSS) in electricity by 14.0 percentage points and the exergy efficiency over the course of 1 year is raised from 33.7% to 36.6%. The SMR-CHP's increased runtime (+39.4%) is a direct result of having to cover the same heat demand with a reduced thermal output power. While this allows it to increase electricity and H_2 production, it also causes the operating costs (i.e., fuel costs) (and CO_2 emissions) to increase significantly (+15.1%). The SMR process should therefore be improved to reach a certain efficiency and as much heat as possible should be recovered and returned to the CHP to better balance pros and cons of SMR integration. In this area, the current SMR configuration shows potential for improvement.

A control logic taking into account not only the TES level but also the actual electricity demand and the operating costs can increase the DSS in electricity for both a conventional and an SMR-CHP system (by 3.8 and 1.7 percentage points respectively). This increase is smaller in case of the SMR-CHP since it already achieves a very high DSS based on extended system runtime without the use of smart dispatching. Furthermore, the relatively long start-up phase of the SMR limits its usability during shorter operation intervals, which should also be addressed in future investigations. Overall, the improved control logic works best during periods of medium to low heat demand and frequent occurrences of electricity demand beyond the break-even point. During winter, operation is largely dictated by heat demand and long operating hours do not leave much room for improvement.

Both the CHP hardware and auxiliary Simulink models (TES and SMR) could successfully be integrated into the Simulation Framework platform thanks to the collaborations described in Section 6. The SFW therefore allowed several hardware-in-the-loop experiments to be conducted despite its early stage of development. Proving the value of the platform and increasing the opportunities for experimental investigation in this task. Thanks to this, the developed control algorithm could be tested with CHP hardware and real-life demand data from NEST, thus showing that the controller is also applicable under less idealised conditions when utilising a suitable moving average filter.

In order to validate the chemical performance of the SMR model used for the simulations mentioned above, a robustly functioning SMR-CHP plant needs to be installed and investigated. The components used within this task are not able to withstand the rough conditions in the exhaust gas path of the present single cylinder engine. Either dampening volumes must be sized and installed, a multi cylinder engine CHP plant should be used, other reformer manufacturers should be reached out to or a combination of the afore mentioned measures should be considered. In the system itself, the following constructive and operational measures need to be taken in order to improve the robustness and applicability of the system:

1. Implementation of a pre-pressure regulator before the flare / further usage of the syngas in order to have a steady pressure in the system even at very small flow rates.
2. The system should be started up only with water flow before a certain process temperature after the reformer is reached and only then methane shall be added to the process.
3. Implementation of an exhaust bypass line such that the exhaust gas can be piped directly into the CHP exhaust gas heat exchanger without flowing through the reformer complex; this will allow for high thermal power production at times when this is necessary.

A number of micro-CHP plants are available on the commercial market, which are similar in size to the Aladin II prototype used here and meet both the requirements for installation at NEST and for an SMR retrofit. Manufacturers or distributors whose products would be particularly suited and who have

expressed interest in collaborating on future investigations are highlighted in the results, Section 3.6. Among these, the Smartblock 7.5 micro-CHP is particularly notable for its capability of coping with hydrogen enriched fuels and the manufacturer's interest in testing the SMR-CHP concept. Due to the tolerance for hydrogen enriched fuels, the produced syngas may, in this case, also be directly used in the CHP and thus lower its net fuel consumption.

5 Outlook and Next Steps

As mentioned in the conclusions, it will be essential for all future simulation investigations to validate (and improve) the SMR model. Therefore, it is highly recommended to build a new laboratory test bench. First, the revised prototype plant must prove the mechanical integrity of the system components by getting rid of the exhaust gas pulsations or featuring more robust reformer components. Secondly, all three improvements proposed in the conclusions must be integrated in the revised version. With this lab-scale plant, the SMR process shall be characterized and then optimized. Once a laboratory plant is running safely and reliably, the SMR concept should be transferred to a commercially available CHP plant as proposed in Section 3.6 to demonstrate the applicability in practice and to investigate the long-term durability of the system. With such a long-term experiment in a realistic environment, the economic viability shall be quantified and compared to a conventional CHP system. Furthermore, the different options for syngas usage shall be investigated. Especially the economic impact of, e.g., purification processes for injection into the gas grid will be of interest when looking at an overall economic analysis of the system.

For the purpose of operational flexibility improvements, cost savings, etc., a whole number of other CHP operation strategies have been suggested by literature (e.g., [20] [24] [2]). A direct comparison of the novel hybrid approach presented in this report with other strategies from literature might thus be appropriate. A recommendation made by Hawkes and Leach [24] to adjust operating strategies seasonally could further improve upon the hybrid control approach. While the current set of thresholds has been shown to work well in spring and autumn, using another set for winter or summer operation might yield additional benefits. Additional simulative investigations should also be conducted to test the sensitivity of the strategy's performance to changing boundary conditions. Hawkes and Leach [24], for instance, have reported high sensitivity of their results to electricity buy-back rates. A study of the effect of different pricing schemes, perhaps outside the setting of a single-family home's private consumer, could thus be of interest. Changing perspective from a single CHP unit to that of a utility or energy provider could be of greater interest for shaping the future energy system.

In that context, HIL simulations combining a multitude of CHP models and, if possible, hardware could be used to investigate and characterise the performance of virtual power plants and develop or adapt suitable dispatching algorithms for the scenario. This would require the CHP Simulink model, developed in this task, to be adapted for the SFW. Furthermore, it would have to be integrated in a way that allows several instances of the model to be used in parallel. The linearized CHP model, described in Section 2.6.3, might alternatively be adapted for this purpose, as it is far less computationally expensive and could be converted to run in python directly.

If research is continued with a commercially available CHP that does not require constant supervision when operating, control algorithms could be tested under realistic conditions in long-term HIL experiments. These may be more insightful than the short-term HIL experiments conducted here and could confirm the behaviour observed in the long-term simulations.

6 National and International Cooperation

The cooperation and collaboration with several institutions and companies was essential to integrate the Aladin II CHP prototype into the SFW and enable hardware-in-the-loop experiments. The CHP was virtually linked to Empa's ehub with great support from the ehub group (see Section 2.7.2). Super Computing Systems AG (SCS) engineered, programmed and maintained the crucial interconnection between the CHP hardware, the SFW software and the external data archive. The last of which was provided by Venios GmbH from Germany along with technical support. And last but not least, the SFW software was developed and provided by ETH's Research Centre for Energy Networks (FEN) along with a lot of effort to accommodate the needs of the investigations presented in this report during early stages of SFW development.

The planning and sizing procedure for the SMR prototype was conducted in cooperation with Bosal ECI who also supplied the necessary heat exchangers and reaction core (see Section 2.4.2).

7 References

[1] M. Staubli, C. Onder, K. Boulouchos, C. Schürch and T. Zobel, “Aladin II – Entwicklung eines Gasbetriebenen, Hochflexiblen „Near-Zero“ Emission Mikro-Blockheizkraftwerks,” SFOE, Bern, 2019.

[2] C. D. Ummenhofer, G. Heyer, T. Roediger, J. Olsen and J. Page, “Improved system control logic for an MCHP system incorporating electric storage,” *Applied Energy,* vol. 203, p. 737–751, 10 2017.

[3] Empa, “NEST Booklet,” [Online]. Available: https://www.empa.ch/documents/56024/11666357/NEST_Booklet_2020_DE.pdf/26b8be99-8f9b-4acc-b3a3-49e5eb13716b. [Accessed 19 01 2021].

[4] C. Schürch, T. Zobel, A. Asani, M. Moisi and M. Staubli, *Aladin II Aufbau und Betrieb von fünf Prototypenanlagen eines gasbetriebenen, hochflexiblen, ``near-zero Emission'' Klein-BHKW,* 2019.

[5] T. Zobel, C. Schürch, K. Boulouchos and C. Onder, “Reduction of Cold-Start Emissions for a Micro Combined Heat and Power Plant,” 2020.

[6] A. C. Celador, M. Odriozola and J. M. Sala, “Implications of the modelling of stratified hot water storage tanks in the simulation of CHP plants,” *Energy Conversion and Management,* vol. 52, pp. 3018-3026, 2011.

[7] P. Vögelin, “Characterisation and optimisation of gas engine combined heat and power plants in a volatile energy system,” 2017.

[8] C. D. Ummenhofer, J. Olsen and T. Roediger, “Partitioning of MCHP-TES system run time to incorporate transient system behaviour: a comprehensive exergy-based analysis using simulation,” *International Journal Energy Research,* vol. 40, p. 1255–1270, 2 2016.

[9] Empa, “Erweiterter Thermischer Response Test und Temperaturmessung,” Eidgenössische Materialprüfungs- und Forschungsanstalt, Dübendorf, 2015.

[10] A. Gerber, “Potential of Seasonal Heat Storage in Combination with a mCHP and a Heat Pump,” Laboratory for Aerothermochemistry and Combustion Systems, ETH Zürich, Zürich, 2019.

[11] KIT, “DETCHEM Chemical reaction mechanisms,” [Online]. Available: https://www.detchem.com/mechanisms. [Accessed 11 2 2019].

[12] L. Croce, “Modelling and Dimensioning of a Steam Reforming CHP Process,” Laboratory for Aerothermochemistry and Combustion Systems, ETH Zürich, Zürich, 2019.

[13] I. Dincer and M. A. Rosen, Exergy: energy, environment and sustainable development, Elsevier, 2013.

[14] İ. Dinçer and M. A. Rosen, “Thermal Energy Storage,” Wiley, 2010, p. 239–242.

[15] V. N. A. Sapkota, “Analysis of Steam Methane Reformer-CHP,” Laboratory for Aerothermochemistry and Combustion Systems, ETH Zürich, Zürich, 2020.

[16] D. Wang, J. Landolt, G. Mavromatidis, K. Orehounig and J. Carmeliet, “CESAR: A bottom-up building stock modelling tool for Switzerland to address sustainable energy transformation strategies,” *Energy and Buildings,* vol. 169, p. 9–26, 6 2018.

[17] “SIA 2024, Standard-Nutzungsbedingungen für Energie- und Gebäudetechnik,” 2006.

[18] Elektrizitätswerk der Stadt Zürich, E. W. Z., “Stromtarif 2019 - Stadt Zürich,” 01 01 2019. [Online]. Available: https://www.ewz.ch/webportal/de/private/strom/tarife/tarifuebersicht.html. [Accessed 19 06 2019].

[19] Energie 360°, A. G., “Preisliste Erdgas und Biogas,” 01 04 2019. [Online]. Available: https://www.energie360.ch/de/energie-360/wissen/erdgas-biogas/gaspreise/. [Accessed 19 06 2019].

[20] D. Haeseldonckx, L. Peeters, L. Helsen and W. D'haeseleer, “The impact of thermal storage on the operational behaviour of residential CHP facilities and the overall CO2 emissions,” *Renewable and Sustainable Energy Reviews,* vol. 11, pp. 1227-1243, 2007.

[21] The Swiss Federal Council, “Ordinance on Air Pollution Control (OAPC),” 16 12 1985. [Online]. Available: https://www.admin.ch/opc/en/classified-compilation/19850321/index.html. [Accessed 19 01 2021].

[22] A. Loose, H. Drück, N. Hanke and F. Thole, “Field Test and Performance Monitoring of Combined Solar Thermal and Heat Pump Systems,” in *ISES Solar World Congress*, 2011.

[23] T. Başer and J. S. McCartney, “Thermal energy storage in borehole heat exchanger arrays,” in *International Symposium on Energy Geotechnics*, Barcelona, 2015.

[24] A. D. Hawkes and M. A. Leach, “Cost-effective operating strategy for residential micro-combined heat and power,” *Energy,* vol. 32, p. 711–723, 5 2007.

8 Appendix

8.1 Schematic of the conventional CHP

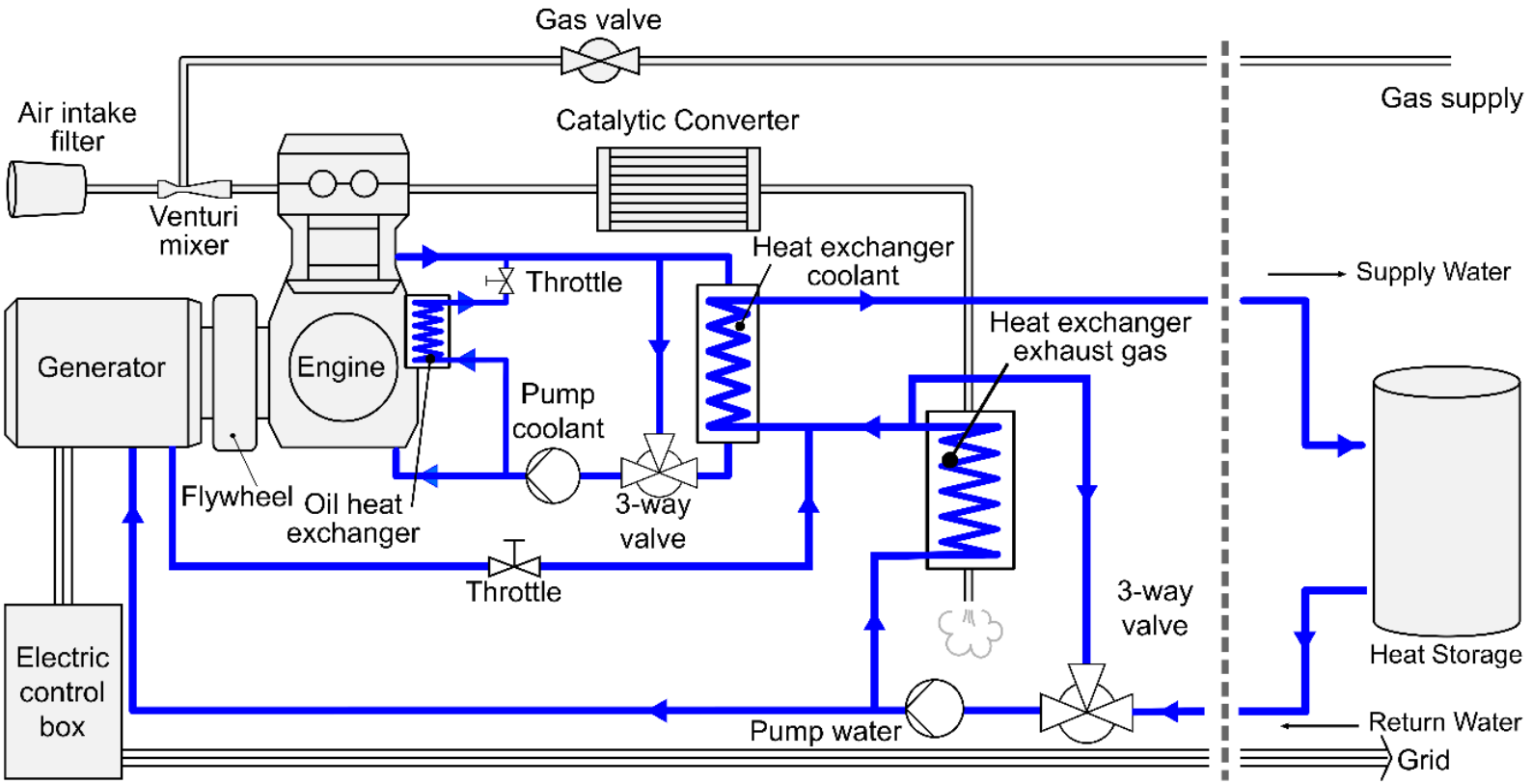

Figure 32: Schematic of the conventional CHP plant, taken from (1). Two cooling circuits transfer the heat from the engine, the oil, the generator and the exhaust to the consumer. The shown heat storage tank is not part of the CHP plant.

8.2 P&ID of the SMR

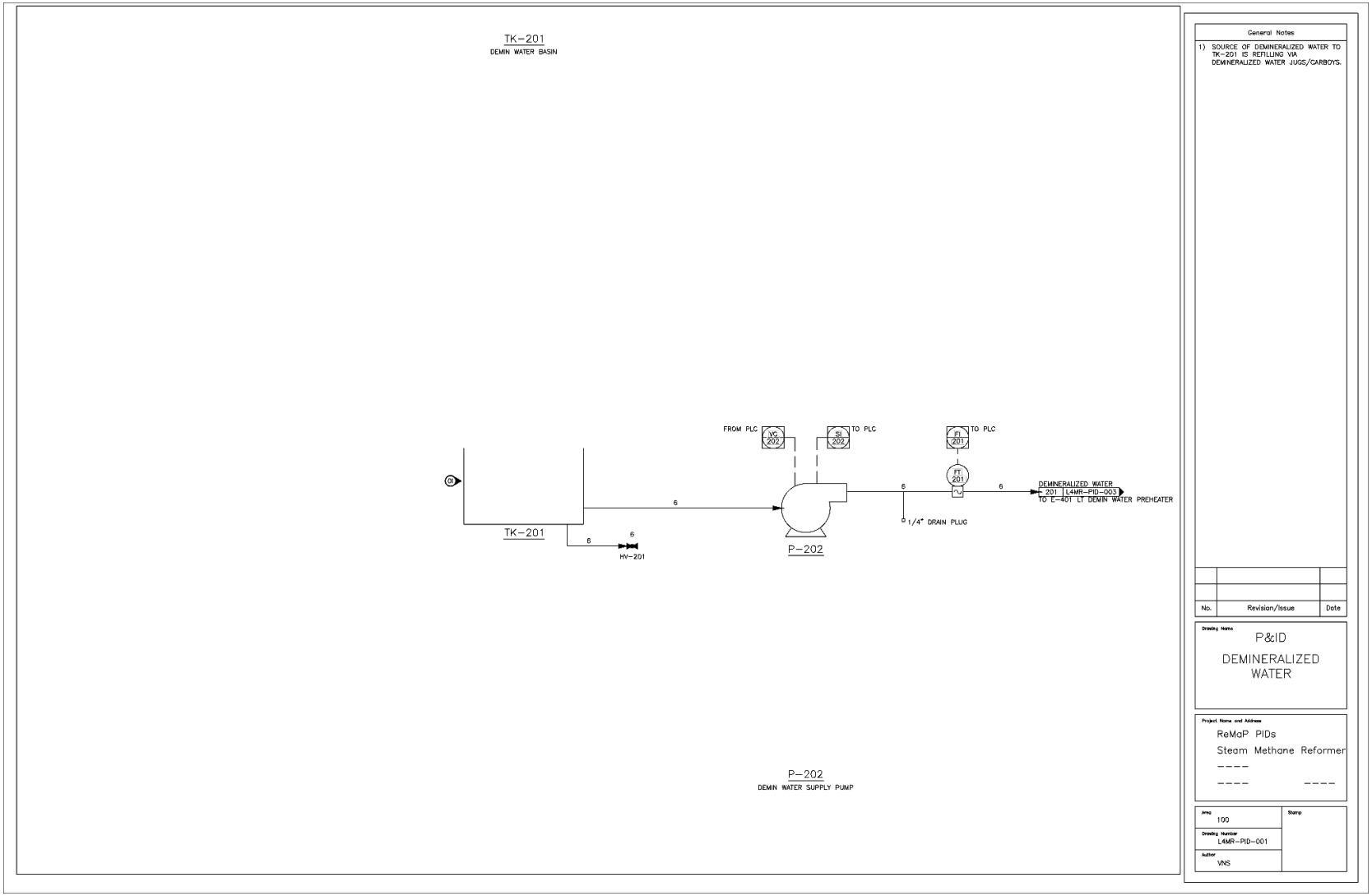

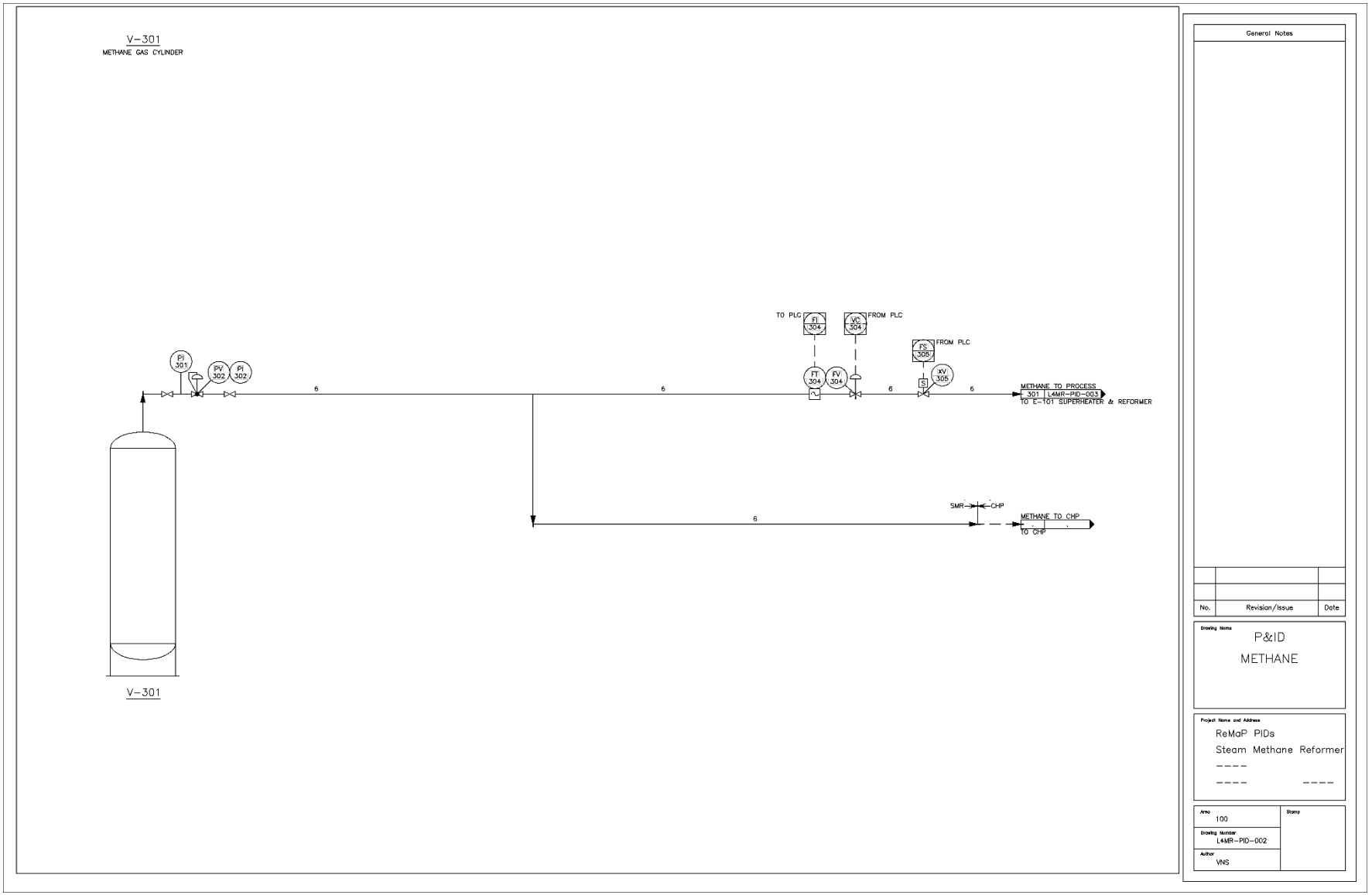
V-301
METHANE GAS CYLINDER
PI 301
PV 302
PI 302
6
6
TO PLC
FI 304
VC 304
FROM PLC
FS 305
FROM PLC
FT 304
FV 304
S
XV 305
6
6
METHANE TO PROCESS
301 L4MR-PID-003
TO E-101 SUPERHEATER & REFORMER
SMR
CHP
6
METHANE TO CHP
TO CHP
V-301
General Notes
No.
Revision/Issue
Date
Drawing Name
P&ID
METHANE
Project Name and Address
ReMaP PIDs
Steam Methane Reformer
Area
100
Drawing Number
L4MR-PID-002
Author
VNS
Stamp

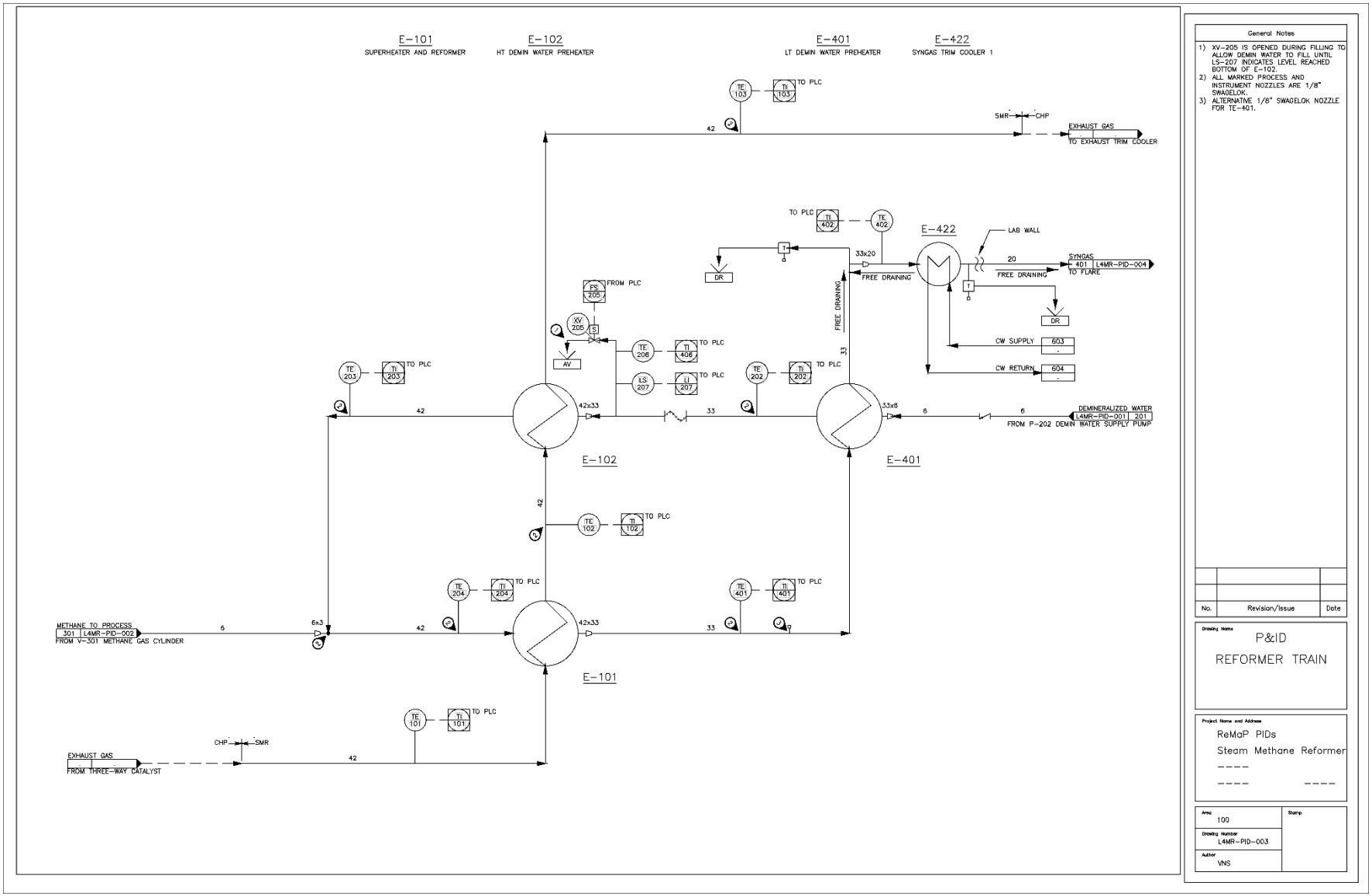

General Notes

1) XV-205 IS OPENED DURING FILLING TO ALLOW DEMIN WATER TO FILL UNTIL LS-207 INDICATES LEVEL REACHED BOTTOM OF E-102.
2) ALL MARKED PROCESS AND INSTRUMENT NOZZLES ARE 1/8" SWAGELOK.
3) ALTERNATIVE 1/8" SWAGELOK NOZZLE FOR TE-401.

No.	Revision/Issue	Date

Drawing Name
P&ID
REFORMER TRAIN

Project Name and Address
ReMaP PIDs
Steam Methane Reformer

Area	Stamp
100	
Drawing Number: L4MR-PID-003	
Author: VNS	

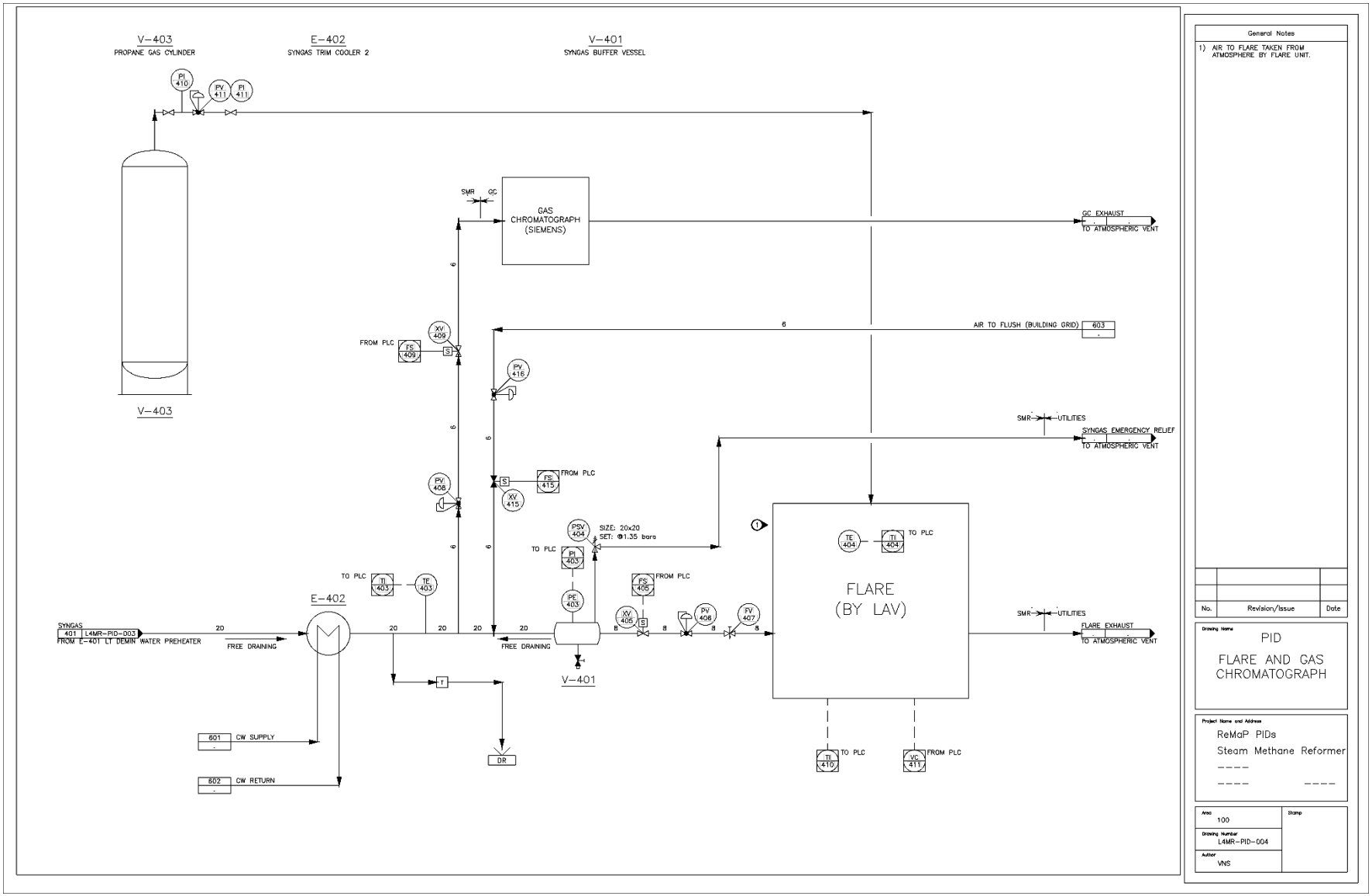
V-403
PROPANE GAS CYLINDER
E-402
SYNGAS TRIM COOLER 2
V-401
SYNGAS BUFFER VESSEL
PI 410
PV 411
FI 411
V-403
SMR
QC
GAS CHROMATOGRAPH (SIEMENS)
QC EXHAUST
TO ATMOSPHERIC VENT
AIR TO FLUSH (BUILDING GRID)
603
FROM PLC
XV 409
FS 409
PV 416
SMR
UTILITIES
SYNGAS EMERGENCY RELIEF
TO ATMOSPHERIC VENT
PV 408
FROM PLC
FS 415
XV 415
PSV 404
SIZE: 20x20
SET: @1.35 bara
TO PLC
PI 403
TO PLC
TI 403
TE 403
E-402
FROM PLC
FS 405
PE 403
XV 406
PV 406
FV 407
FLARE
(BY LAV)
TO PLC
TE 404
TI 404
SMR
UTILITIES
FLARE EXHAUST
TO ATMOSPHERIC VENT
SYNGAS
401
L4MR-PID-003
FROM E-401 LT DEMIN WATER PREHEATER
FREE DRAINING
FREE DRAINING
V-401
T
DR
601
CW SUPPLY
602
CW RETURN
TI 410
TO PLC
VC 411
FROM PLC
General Notes
1) AIR TO FLARE TAKEN FROM ATMOSPHERE BY FLARE UNIT.
No.
Revision/Issue
Date
Drawing Name
PID
FLARE AND GAS CHROMATOGRAPH
Project Name and Address
ReMaP PIDs
Steam Methane Reformer
Area
100
Drawing Number
L4MR-PID-004
Author
VNS
Stamp